Numerical comparison of an office cooled with and without a ventilated slab using a model predictive controller

Matthieu Labat, Ion Hazyuk

Numerical comparison of an office cooled with and without a ventilated slab using a Model Predictive Controller

Matthieu Labat*[1], Ion Hazyuk[2]

[1] LMDC, INSA/UPS Génie Civil, 135 Avenue de Rangueil, 31077 Toulouse cedex 04 France.

[2] Institut Clément Ader, Université de Toulouse, INSA/ISAE-SUPAERO/MINES-ALBI/UPS/CNRS, 31400 Toulouse, France

*Corresponding author: m_labat@insa-toulouse.fr

Abstract

Ventilated slabs are Thermally Activated Building Systems (TABS) that use the supply air as the heating/cooling medium for taking advantage of the thermal inertia of a slab. The objective for the ventilated slab is to maintain the indoor temperature within the desired range for a minimal energy consumption, at least equal or lower than with a regular (non-ventilated) slab. To achieve such objectives, an efficient control is required but the latter is challenging for TABS because of the delay brought by their thermal inertia. While advanced control techniques are available and suitable with TABS, it is not always clear if the final performances are driven by the control technique itself or the inherent thermal potential of the ventilated slab. The present paper numerically analyses the behaviour of the ventilated slabs controlled with a Model Predictive Controller, and provides a comparison with a non-ventilated slab combined with the same controller. This comparison was extended to four other airflow rates, since it significantly changes the thermal dynamic of a ventilated slab. The indoor temperature requirements were satisfied most of the time and energy demand differences observed between the two systems were minor. However, a lower airflow rate is preferable as it decreases the consumption of the fans, which was significant for this test case. The most important improvement brought by the ventilated slab was the smoothed temperature variation

at the outlet of the slab, resulting in a smaller blown air – room air temperature difference with ventilated slabs and thus favouring indoor comfort.

Keywords:

Thermally Activated Building Systems, Model Predictive Controller, Energy demand, Modelling, Building

Nomenclature

Latin Symbols	Description	Unit
A, B, C, D	Matrices of the state space model	-
C_p	Specific heat capacity	$J.kg^{-1}.K^{-1}$
C_{th}	Total heat capacity	$J.K^{-1}$
E	Energy	kWh
e	Thickness	m
f	Cost function	-
G_v	Indoor vapour production	$kg_v.s^{-1}$
HIR^*	Hygric Inertia of the Room	$kg.m^{-3}.\%\ RH^{-1}$
I	Furniture density	$kg.m^{-2}$
k	Thermal conductivity	$W.m^{-1}.K^{-1}$
L_v	Latent heat capacity of water	$J.kg^{-1}$
$\dot{m}$	Mass flow rate	$kg.s^{-1}$
p	Pressure	Pa
P	Power	kW
$\dot{Q}$	Heat flux	W
Q_v	Volumetric flow rate	$m^3.s^{-1}$
r	Moisture content	$kg_v.kg_A^{-1}$
R_{th}	Thermal resistance	$K.W^{-1}$
R_v	Gas constant for water vapour	$J.kg^{-1}.K^{-1}$
S	Surface	m^2
T	Temperature	°C
t	Time	s

U	Overall heat transfer coefficient	$W.m^{-2}.K^{-1}$
V	Volume	m^3

Greek Symbols

α	Penalty coefficient	-
θ	Temperature exceedance	°C.h
η	Efficiency	-
λ	Size of the population	-
ρ	Density	$kg.m^{-3}$
ρ_P	Pearson's coefficient	-
σ	Standard deviation	-
τ	Fraction of air flow	-

Subscripts

a	Air
B	Blown
c	Convection
f	Floor
in	Inlet of the slab
L	Heat load
Low	Lower threshold
o	Overlapping
$Room$	Room
s	Span (of the time window)
T	Transmitted
Up	Upper threshold
W	Wall
Wa	Water

Upper scripts

$\bar{}$	Mean value

Acronyms

ACH	Air Change per Hour
BAS	Building Automation System
COP	Coefficient Of Performance
GA	Genetic Algorithm
HVAC	Heating Ventilation and Air Conditioning

MAE	Mean Absolute Error
MPC	Model Predictive Controllers
NVS	Non-Ventilated Slab
RE	Relative Error
TABS	Thermally Activated Building Systems
VS	Ventilated Slab

1. Introduction

1.1. On the use of thermal inertia to cope with warm outdoor conditions

Because of climate change and population growth, the cooling demand in buildings is bound to increase dramatically during this century [1]. This motivates the research and development of cooling techniques that are able to provide comfortable indoor conditions during summer at the lowest possible energy cost. Among the numerous possible solutions [2,3], promoting thermal inertia has proved to be an effective means of limiting high indoor temperatures when it is combined with free cooling (also known as night ventilation) [4]. The basic concept is that the thermal mass of the building delays the occurrence of peak temperature from the daytime, when solar radiation and indoor heat loads are high, to the evening, when the outdoor temperature decreases. Increasing the air change rate during the night, by means of window opening or an increase in the fan speed, helps to remove the heat stored during the day for a relatively low energy consumption. In reality however, it might not be easy to provide comfortable indoor conditions by this means alone, e.g. because the heat loads of the buildings are too high. Therefore, it is likely that night ventilation will need to be coupled with conventional cooling techniques, yet operating both strategies simultaneously raises questions in terms of energy consumption, as underlined in [5]. The second difficulty is that increasing the mass of a building significantly impacts the structure of the building. Moreover, using the thermal inertia of the building structure is not straightforward because of its passive nature and the increase in mass could even lead to worse indoor conditions compared to lightweight buildings

[6]. For this reason, active solutions, known as Thermally Activated Building Systems (TABS), have been developed recently to further develop cooling strategies based on thermal inertia.

TABS are building elements that are actively used for heat transfer and heat storage. Water pipes or air ducts are embedded in the building surfaces or in the building structure to work as heat exchangers, transferring heat to the rooms of the building and storing thermal energy in the structure [7]. It is now recognized that TABS are effective in improving indoor environmental quality compared to conventional air systems. They take advantage of radiative heat transfer, which limits the airflow rate that has to be supplied and also the air temperature that is required for providing comfortable indoor conditions [8]. Among these systems, ventilated slabs (or hollow core slabs) differs from others because they use the supply air as the heating/cooling medium instead of requiring two separate thermal systems (TABS and supply air flow).

Ventilated slabs can be seen as a system that provide two different heat fluxes to the room: the first one is transmitted through the slab to the room with a significant delay due to the thermal mass of the slab. It achieves the main purpose of TABS and allows energy strategies that relies on thermal inertia. The second heat flux, that is blown at the outlet of the slab into the room, is provided immediately to the room but the temperature of the air blown differs from the one at the inlet of the slab because of the heat storage within the slab. Compared to the transmitted heat flux, it allows providing a faster response to sudden indoor temperature variations. However, its intensity is hard to determine since it depends on the thermal history of the slab. Such systems have already been studied by others over recent decades [9,10], where detailed physical based model were used to provide an exhaustive understanding of the thermal behaviour of such systems. Most of the time, such studies rely on simple boundary conditions and parametric runs to determine the influence of the design parameters (e.g. number and spacing of embedded ducts, thickness and length of the slab, airflow rate). To explore the behaviour of these systems for various and dynamic boundary

conditions more easily, numerical techniques have to be used in order to obtain a lighter model of the ventilated slabs such as exemplified in [11,12].

1.2. Significance of using Model Predictive Controllers with TABS

While TABS design remains simple, their control is still a major challenge [7]. The TABS slow response time makes it harder to maintain the indoor temperature within a narrow range under time varying heat loads. Classical control techniques (such as on/off controller, weather compensating control, or PID controller) could then lead to discomfort. It has even been reported [13] that inappropriate control for TABS can lead to a significant increase in energy consumption by the HVAC system (Heating Ventilation and Air Conditioning) as it switches between heating and cooling modes in a very short time frame. A similar conclusion was obtained during earlier work [12], which stressed the need to apply advanced control techniques to a ventilated slab.

Among the different techniques used for control, Model Predictive Controllers (MPC) are good candidates for HVAC systems including TABS, according to [14,15]. It has also been applied to a wide range of lighter thermal building systems, such as floor heating [16,17], and demonstrates good performances when applied to real buildings [18]. A predictive controller calculates the optimal control signal over a future time span (or receding horizon), which optimizes a given cost function, e.g. the overall energy consumption, the set-point deviation, or a combination of the two. The optimization relies on simulating the system over a relatively short receding horizon, so the computational cost remains low. Two main families of MPC can be distinguished: online and offline. For online MPC, once the optimization is completed for the current time window, the first value of the control sequence is applied to the system and the optimization is repeated for the next time window. The advantage of online MPC is that each time a new optimization starts, the measured values are updated and used, which can compensate for a modelling mismatch or inaccurate input such as forecasted weather conditions. However, its main drawback is the computational burden,

especially when large scale problems, short sampling periods and commercial applications are concerned. Offline MPC is designed to mitigate this problem. It transforms the online optimization problem into an explicit solution in the form of a piecewise affine state-feedback control law. During operation, the feedback gains are obtained from a look-up table based on the actual state vector. The look-up table itself is computed by a single optimization run, which can be done offline. Thus, the time-consuming and complex optimization is carried out offline, and the controller implementation uses a simple look-up table plus a vector multiplication. Given that the optimization is carried out only once, this technique is well suited to situations where the set-point and disturbance prediction during operation are the same as in optimization. For building thermal control applications this might hold for the set-point, but not for forecasting weather and internal loads.

Although not intended to be implemented on the real system, another application of MPC is to assess the best possible potential of a given set-up. This is relevant if a base case is needed for the evaluation of different control strategies [19] or if the full potentials of two different system set-ups (not the control algorithms) are to be compared. In this case, the optimization problem can be settled as for online MPC, but carried out only once. This supposes that disturbance predictions are perfectly known and there is no mismatch between the model and the system. This technique is suitable when the aim is to better understand the behaviour of a complex system and search for its optimal command. To ensure that the optimization problem is tractable, a long simulation time can be broken down into shorter prediction horizons. Thus, the search space is smaller and suitable for use with optimization techniques. The main drawback is the reliance on modelling alone, which means that the improvements obtained by the optimized command are questionable as they depend on the quality of the model.

Some examples can be found in [16,20] for a hydronic system and in [11] for a ventilated slab. To the best of our knowledge, [11] is the sole example of advanced control techniques applied to ventilated slabs. A comparative analysis was carried out to evaluate the impact of ventilated slab

systems' design properties on the optimal operational cost savings. It was found that operating a precooling strategy prior to occupancy could reduce the cost of operation if the ratio of on-peak to off-peak was high enough (≥ 3) when compared to conventional night set-up control. The influence of the mass flow rate on the strategy was not discussed, the latter having a major influence on the dynamic of the system however according to [9,21]. Second, it was not always clear if the overall good performances can be attributed to the ventilated slab itself or to the control technique. A comparison with another classical system using the same control technique would contribute in discussing the merits of the ventilated slabs.

1.3. Objective and methodology

A mentioned above, the objective for the ventilated slab is to maintain the indoor temperature within the desired range for a minimal energy demand. The latter should be at least equal or lower than with a regular (non-ventilated) slab. The present paper stands a contribution to the study of ventilated slabs and proposes to further analyse the pros of ventilated slabs. It is restricted to the case study of an office room during summer, where the cooling demand is generally high and the heating demand is low or even non-existent.

The ventilated slab will be modelled under the constraint of a constant airflow rate, but the simulation work will be repeated for various airflow rates. In order to prevent any bias in this comparison, identical boundary conditions should be used for both systems. It means that the same heat load will be applied to the room and that case with a non-ventilated slab will be optimised by using the same technique. Since the performance of TABS are highly dependent on the controller used, the same controller will be applied to both systems. This allows considering the relative rather than absolute performances of the ventilated slab. While the merits of the MPC controller still remain to be proved compared to simpler controllers [22], especially from the practical application standpoint, it was kept in the present study because of its evident advantages for a TABS system. An

offline approach is used since the objective is to assess the maximal potential of the ventilated slab as compared to a classical system. Although the application of predictive controllers still remains a challenge, this study aims at comparing both slabs with a control algorithm able to take the greatest advantage of thermal inertia.

The methodology for modelling is presented in Figure 1. The model of the physical system will be detailed in section 2 and can be broken down in four parts (light grey boxes and solid lines in Figure 1):

1. The ventilated slab itself is modelled by means of a state space model. It relies on the work presented in [12] and will be briefly summarized here. It uses the air temperature at its inlet, T_{in}, and the room temperature, T_{Room}, as inputs;
2. The room, whose temperature T_{Room} is controlled, is simply modelled by means of heat and mass (water vapour) balances;
3. Hourly weather data and indoor heat load profiles were used as boundary conditions;
4. A simple HVAC system was modelled and rely on heat and mass balances. It aims at estimating the energy demand that is required to maintain a given temperature set-point, T_{in}, for the air to be blown into the ventilated lab. The detailed elements of the HVAC system (pumps, refrigerating unit, …) were not modelled, nor the local control loops associated to its elements.

The optimization technique and the MPC will be presented in section 3 (dark grey boxes and dashed lines in Figure 1). It relies on:

1. A basic algorithm that uses a Genetic Algorithm (GA). Since the development of MPC or GA is not the objective of the present study, the method will be shortly discussed and the interested reader is invited to read the appendices in section 8 for further details. The output

of the MPC is the temperature setpoint at the outlet of the HVAC system, used as the inlet of the ventilated slab T_{in};

2. An objective function, which is to minimize the energy demand for the HVAC system;
3. A set of constraints, which are defined by the acceptable temperature ranges for T_{Room} and $T_{in.}$

This flow chart is very similar when it comes to deal with a non-ventilated slab. The differences are the following:

1. The air at the output of the HVAC system is used directly as an input for the room heat balance. It corresponds to the fact that the air is blown directly into the room and not into the slab anymore;
2. Another state space model is used for modelling the slab, and uses only the room temperature as an input.

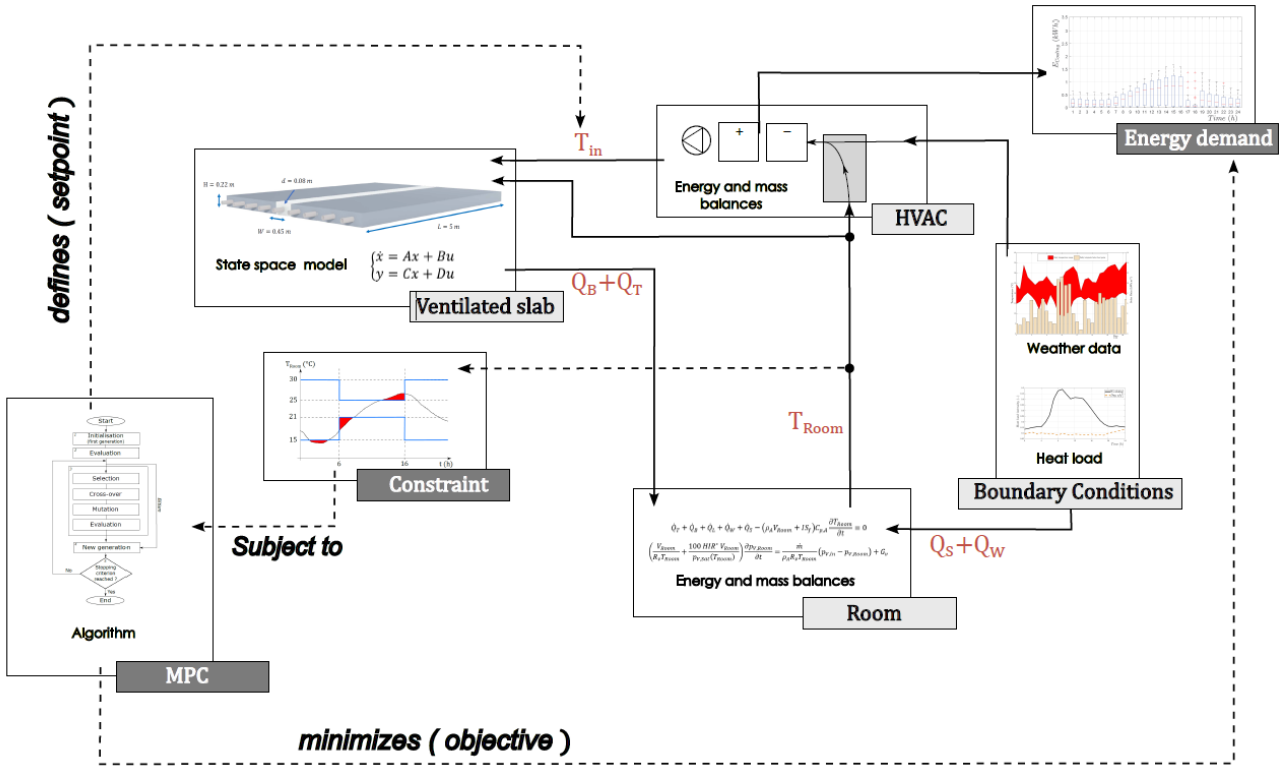

Figure 1 : Flowchart of the proposed methodology.

Finally, since the mass flowrate was found to have a significant influence in an early study, its impact will be evaluated in section 4. These results will be presented and analysed for the two slabs and five different values of the airflow rate.

2. Modelling of heat and mass transfer

In this section, the models of the Ventilated Slab (VS) and Non-Ventilated Slab (NVS) will be presented first. Then, the room heat balance will be presented together with the chosen outdoor conditions and indoor schedule for the heat loads. The fourth part is dedicated to the HVAC system and describes how the energy demand will be estimated. As the energy demand for cooling includes the latent energy for dehumidification and since the HVAC system reuses indoor air, the last part presents a lumped model for computing the indoor mass (water vapour) balance.

2.1. Ventilated slab

The description and the modelling of the ventilated slab were developed in a previous study [12] and are briefly recalled below.

The ventilated slab studied here was inspired by a full-scale commercial prototype built by Vinci and named GreenFloor®. The slab is 5 m long and 0.22 m high, and the diameter of the embedded ducts, *d*, is 0.08 m. The ducts are evenly distributed within the slab, their axes being spaced 0.45 m apart. This design was selected to fit the requirements for classical offices. In practice, the ducts are placed first and the concrete is poured over the whole surface at once. The system modelled here is a 20.25 m^2 slab that involves 9 ducts, as shown in Figure 2.

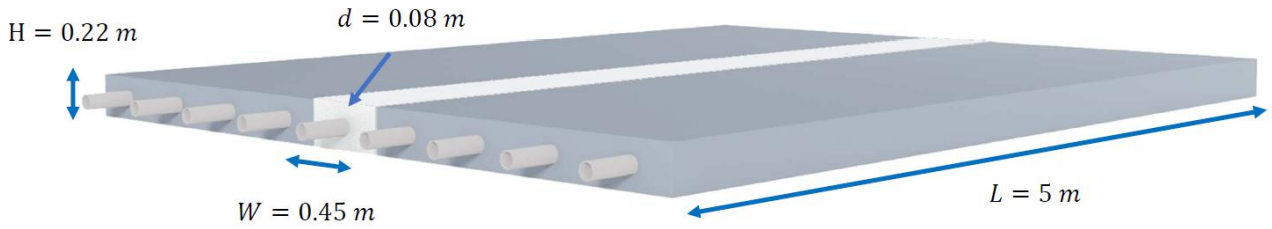

Figure 2 : Scheme of the ventilated slab [12].

Based on detailed 3D finite differences modelling, a reduced model of heat transfer is proposed. It was developed to determine the main heat fluxes exchanged between the slab and the indoor environment with good accuracy but at a much lower computational cost. It came down to a state-space model having the general form:

$$\begin{cases} \dot{x} = Ax + Bu \\ y = Cx + Du \end{cases} \quad (1)$$

where *x* is a column vector containing the state variables, *A*, *B*, *C* and *D* are matrices that contain the parameters of the system model, *u* and *y* are column vectors containing the inputs and the outputs, respectively, defined as:

$$u = [\dot{m}C_{p,a}T_{in}(t) \quad -\dot{m}C_{p,a}T_{Room}(t)]^T \quad (2)$$

$$y = \begin{bmatrix} \dot{Q}_T(t) & \dot{Q}_B(t) \end{bmatrix}^T$$

where $\dot{m}_a$ is the air mass flow rate, $C_{p,a}$ is the specific heat capacity of air (1006 J.kg^{-1}.K^{-1}), T_{in} is the air temperature at the inlet of the ventilated slab, T_{Room} is the room temperature, $\dot{Q}_T$ is the heat flux transmitted to the room by conduction through the slab and $\dot{Q}_B$ is the heat flux blown into the room. VS are designed to be constructed in multi-storey buildings where a single VS is used to deal with one room only, the one that is located below. This is achieved in practice by means of a thermal insulation layer added on its top surface, so that $\dot{Q}_T$ represent the heat flux that leaves the slab through its bottom surface only.

The dimension of the state space model that was proposed is 6. Note that the state variables of the reduced model don't have any physical equivalence. From the mathematical standpoint, they can be seen as a new, smaller basis, on which the full model is projected, with the aim of approximating the system output with less variables. The coefficients of the reduced model were identified from the numerical results obtained with the finite element model. The mean error obtained with the state space model was found to be lower than 0.03 W for a one-month simulation with realistic input variations. The error remained in a ± 36 W interval for the instantaneous heat flux blown into the room when this flux ranged over a ± 900 W interval.

The advantage of using a state space model is that it provides reliable results for a much lower computational cost than solving detailed heat and mass transfer within the slab would, by using a finite element approach, for example. One strong limitation of the proposed model is the use of a constant mass flow rate, since variable air flow rate is now a common technique.

This procedure was repeated for five different air flowrates (300, 250, 200, 150 and 100 m^3.h^{-1}), leading to five different state space models. The values of the coefficients are provided in section 8.5.

2.2. Non-Ventilated slab, or heat transfer within a regular slab

In classical building configurations, the slab is usually non-ventilated. Although not as efficient as a TABS, it can still store and release heat and thus produce a time shift in the peak demand for space cooling. In order to quantify the potential energy savings enabled by the use of the ventilated slab, the base case for comparison will be a regular (non-ventilated) slab. A light dynamic model of the slab is required in order to apply the same control algorithm as with the ventilated slab. It can be obtained by applying a model reduction technique to a 1D finite differences model of the slab. The model reduction method used here and the reduced model are briefly explained in section 8.1 for the sake of clarity.

For the case studied in this paper, the overall geometry of the NVS was the same as for the VS (see Figure 2). For the detailed model, the NVS was cut into 220 layers, so each one was 1 mm thick, providing the same number of state variables. By following the procedure in section 8.1, the model was reduced to only four state variables. The choice of the number of slow states was driven by the estimation error obtained with the reduced model when set against the detailed model. Figure 3 compares the simulation results of the detailed and reduced models for an input corresponding to the outdoor temperature over a period of one year in the south of France. This excitation is richer in terms of frequencies and amplitude compared to typical indoor temperature, so the test is more demanding. As it can be seen in Figure 3, the error lies within ± 2 W while the mean error over the whole period is close to zero. On the other hand, the computational time was reduced by a factor of about 40. The numerical values of the reduced model are given in section 8.6. This reduced model will be used in the following sections to model the non-ventilated slab.

(a)

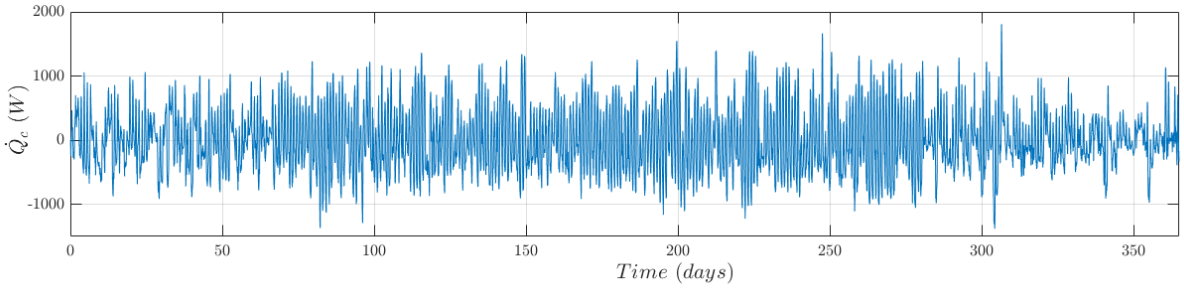

(b)

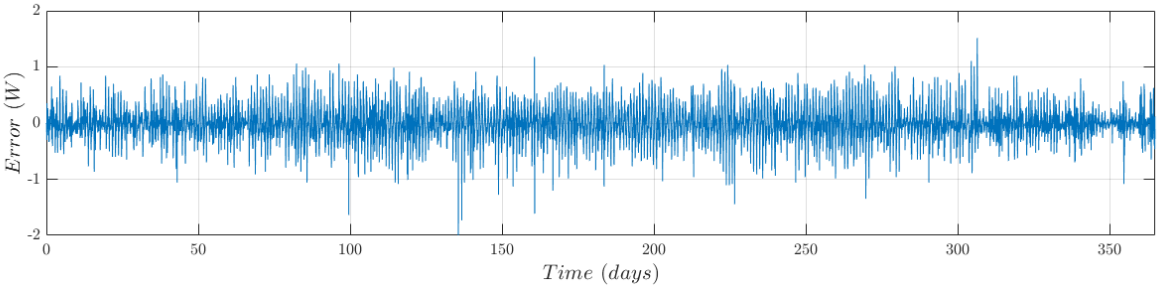

Figure 3 : Heat exchanged between the slab and the room. Results obtained with the detailed model (a) and error obtained with the reduced model (b).

2.3. Indoor heat balance

The heat balance at the room scale gives, for VS:

$$\dot{Q}_T + \dot{Q}_B + \dot{Q}_L + \dot{Q}_W + \dot{Q}_S - \left(\rho_A V_{Room} + IS_f\right) C_{p,A} \frac{\partial T_{Room}}{\partial t} = 0 \quad (3)$$

where $\dot{Q}_L$ is the heat load from occupants, lighting and plug loads (W), $\dot{Q}_W$ is the heat flux through the walls (W), $\dot{Q}_S$ is the solar flux that enters the room through the window (W), S_f is the floor area and I is a coefficient used to take the thermal inertia of the indoor furniture into account.

If a NVS is modelled, equation **(**3) has to be modified as follows:

$$\dot{Q}_c + \dot{Q}_H + \dot{Q}_L + \dot{Q}_W + \dot{Q}_S - \left(\rho_A V_{Room} + IS_f\right) C_{p,A} \frac{\partial T_{Room}}{\partial t} = 0 \quad (4)$$

where $\dot{Q}_c$ is the heat transfer with the NVS (see section 8.1) and $\dot{Q}_H$ is the heat flux provided by the HVAC system directly to the room.

The value of I is set at 40 kg.m^{-2}, which is representative of an office with medium furnishing according to [23]. To be more precise, this value should be multiplied by the specific heat capacity of

the furnishing rather than air. However, the specific heat capacity of air can be considered an acceptable average value for the furnishing materials used and is good enough for approximating indoor thermal inertia. Heat transfer through the wall is evaluated by considering a glazed wall, a common feature of modern high-rise offices. As its mass is rather small compared to that of the slab, its thermal inertia is neglected and the heat transfer can be evaluated as follows:

$$\dot{Q}_W = US_W(T_{Ext} - T_{Room}) \quad (5)$$

where U is an overall heat transfer coefficient set at 1.5 $W.m^{-2}.K^{-1}$, S_w stands for the vertical wall surface area (10.125 m^2) and T_{Ext} is the temperature outdoors.

Since a glazed office was considered in the present study, solar gains were taken into account. Direct and diffuse solar radiation was computed on a tilted (vertical) surface, based on hourly meteorological data obtained on a horizontal surface. This calculation is classical and is detailed in [24], among others. A west-facing orientation was chosen as it corresponds to the most critical case during summer. In fact, solar loads are the highest at the end of the day, when the outdoor temperature is highest and when the thermal inertia of the ventilated slab has already been brought into play. Therefore, the cooling demand is high and it is harder to rely on the thermal inertia alone to provide comfortable indoor conditions. It could be observed that solar heat loads are not instantaneously transferred to indoor air in general, and finer approaches can be found in the literature such as in [25], where an 3D model of the room is used so that the projection of solar radiation through a window onto interior walls and the internal longwave radiative heat transfer were taken into account. For ventilated sab however, as the floor top surface is supposed to be strongly insulated to prevent undesired heat transfer with the ventilated slab located underneath (see Figure 4), the solar heat loads are transferred quickly to the room. It was considered as instantaneous in the modelling.

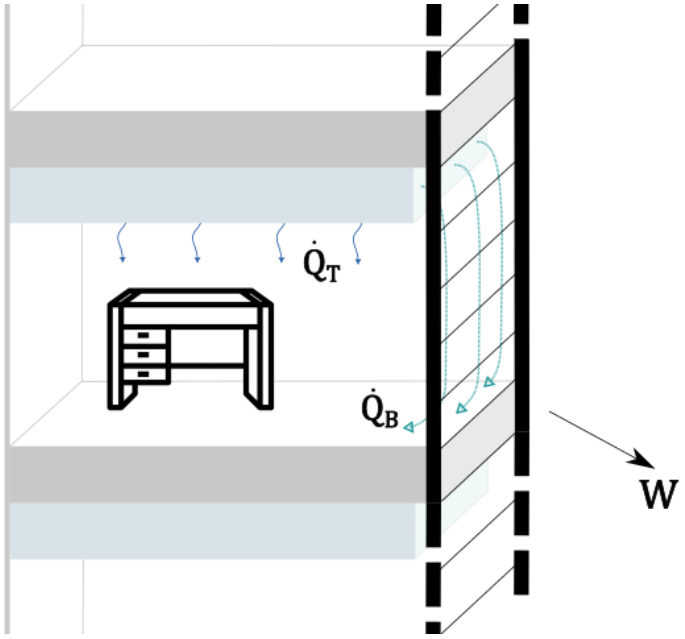

Figure 4 : Basic layout of the simulated office room (ventilated slab in light blue) equipped with a west-oriented glazing wall.

The climatic conditions of Montpellier, France, were selected and are representative of a Mediterranean climate. A 30-day hot period was selected, approximately corresponding to the period defined between mid-July and mid-August. Hourly weather data were used in the present study, and they were processed to present daily values and ranges in Figure 5.

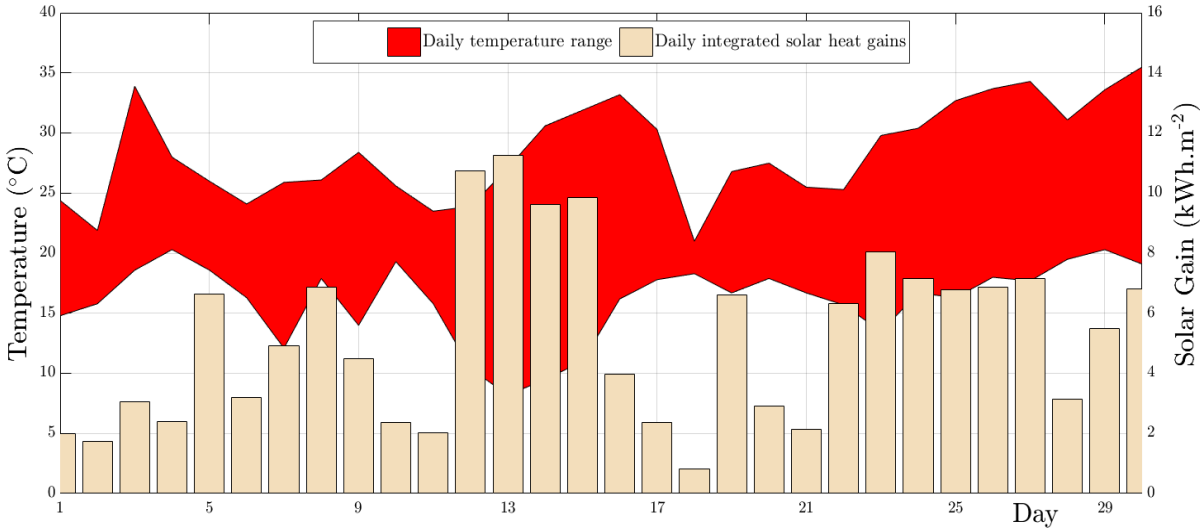

Figure 5 : Daily temperature range (area - left scale) and daily integrated solar heat gains through the vertical west-oriented wall (bars - right scale).

Indoor heat loads result mainly from the occupants' metabolisms, lighting and plug load usages. In the present study, it was decided to take a global value of 24 W.m^{-2} for the peak value of the heat gains. It is recognized that higher values are commonly used by practitioners for sizing HVAC systems (up to 70 W.m^{-2} for offices). However, much lower values (8 W.m^{-2}) were considered by [20] in the context of a large office building, so the value retained in the present study can be considered as realistic. In a certain way, the choice of a rather moderate value for the internal heat loads gives more weight to the outdoor conditions, especially the solar loads.

In addition, a schedule was developed based on metered data from the year 2018 in a research building in Toulouse, in a fashion similar to that proposed by [20]. The electricity demand profiles were averaged from May to the end of June. A distinction was made between weekday and weekend (or day-off) schedules. Both profiles are presented in Figure 6. A low yet positive value can be noted during the night and the weekend. While some very high values were measured punctually, the mean profile never exceeds 50% of the peak value. Therefore, this schedule is realistic but also less demanding than others, some of which consider that all the appliances are turned on during working hours.

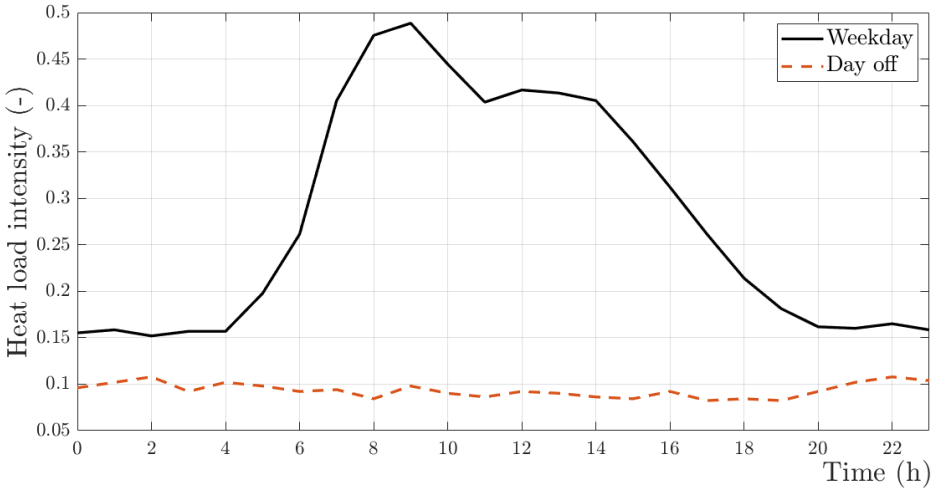

Figure 6 : Sensible heat load intensity schedules for weekdays and days-off (solar time on the abscissa).

The two schedules were then combined in a weekly schedule that included 5 weekdays and two days-off, with 1st January assumed to be a Monday. Transition between the two schedules around midnight was smoothed over 4 hours.

2.4. HVAC system

The HVAC system is depicted in Figure 7. It comprises the following elements, where the numbers in the list correspond to the symbols in Figure 7.

1. An airflow mixer, used so that a fraction of the air leaving the room is reused. The main parameters of this system are the mixing ratios τ_1 and τ_2, the sum of which equals one. The airflow coming from outdoors has to meet the minimum value for air renewal (1 Air Change per Hour (ACH)) but can be increased if this enables energy savings. Details of the modelling and especially of the control logic of the mixing ratios are presented in section 8.2;

   A cooling coil, used if the temperature at the outlet of the mixer (T_M) is higher than T_{in}. It cools the air so that its temperature reaches the targeted value. The main parameter of this system is its efficiency, denoted η. It is used to determine the temperature of the chilled water T_{wa} that has to be supplied in order to meet T_{in}. Assuming a constant water mass flow rate that is high enough, the water temperature between the inlet and outlet remains differs slightly.

The mean value T_{wa} can be used to give an approximation of the moisture content at the inlet of the ventilated slab, r_{in}. An upper limit, r_{Sat}, was added and represents the moisture content of air at a given temperature when relative humidity is unity.

$$T_{wa} = T_M + \frac{(T_{in} - T_M)}{\eta} \tag{6}$$

$$r_{in} = min\left(r_M - max\left(0; \eta\left(r_M - r_{Sat}(T_{wa})\right)\right); r_{Sat}(T_{in})\right) \tag{7}$$

When there is no cooling demand, *i.e.* when T_{in} is higher than T_M, the moisture content remains the same but equations (6) and (7) are still valid. The water temperature could be obtained from a mixing valve placed on the chilled water network, provided that the minimal temperature of the network meets the requirement of the system. As this study is focused on the air conditioning system, the network was not modelled but it was assumed that it allowed T_{wa} to be obtained instantaneously;

2. An electric heating coil, used when T_M is lower than T_{in}. This should happen mostly at interseason and during winter, almost never in summer;
3. A supply fan, blowing air into the ventilated slab at a constant flowrate;
4. The ventilated slab and the room, which were modelled together. For the sake of clarity, some of the heat fluxes that participate in the heat balance (see equation (3)) are not presented in Figure 7;
5. A return air fan, which extracts air from the room at the same mass flow rate as it is introduced by the supply fan and pushes it toward the airflow mixer. The air finally leaves the HVAC system at temperature T_e.

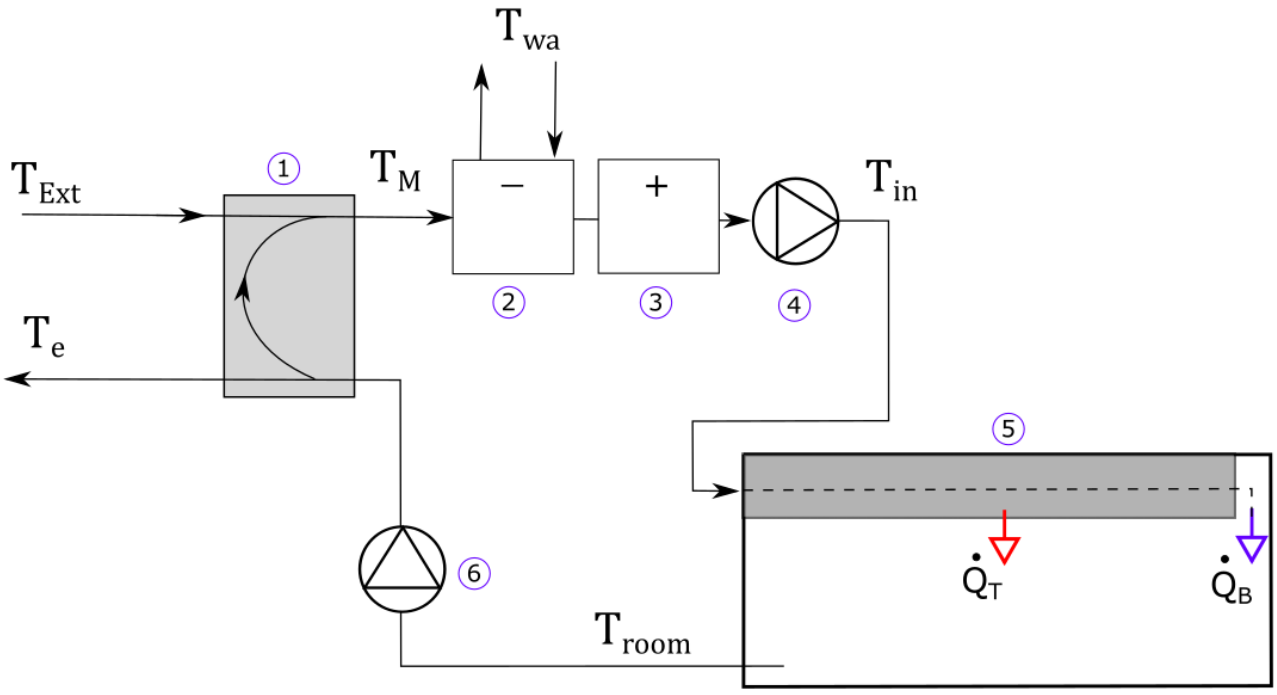

Figure 7 : Scheme of the HVAC system combined with a ventilated slab to control the room temperature (T_{room}).

In a first stage, the energy demand was estimated by considering the power demand of the cooling and heating coils only. While the power demand of the two fans is not negligible, it can be determined easily since a constant airflow rate will be used. Thus, it does not depend on the operation of the system, which is the pattern of the temperature set point for T_{in}. This is the crucial point of this study and will therefore be estimated later. The cooling and heating power demand were estimated by applying the energy balance to air when it flows through the cooling and heating coils. It was assumed that the two coils are never used simultaneously, and the energy balance gives:

$$P = \dot{m}\left(C_{p,a}(T_{in} - T_M) + C_{p,v}(r_{in}T_{in} - r_M T_M) + L_v(r_{in} - r_M)\right) \quad (8)$$

where r is the moisture content of air ($kg_v.kg_A^{-1}$), $C_{p,v}$ is the specific heat of water vapour (1820 $J.kg_v^{-1}.K^{-1}$) and L_v is the latent heat of water vapour (2501.6 $kJ.kg_A^{-1}$).

Equation (8) gives positive values for heating and negative values for cooling. The moisture content remains constant for heating but can decrease for cooling (see (7)), introducing an additional energy demand for dehumidifying often called latent energy.

Since an electric coil is used for heating, the energy demand equals the heating demand. Assuming that the chilled water network is supplied by a refrigerating unit, the energy demand differs from the cooling demand because of the Coefficient Of Performance (COP) of the unit:

$$E_{Cooling} = \int_{o}^{t} \frac{P}{COP(T_{Ext})} dt \quad (9)$$

Where $E_{Cooling}$ is the energy demand for cooling (Wh).

While the Coefficient Of Performance (COP) is specific to a refrigerating unit, it is well known that the COP of an air to water system depends on the outdoor temperature, its value decreasing when the temperature of the outside environment rises. Here, we propose to simply model the COP as a linear function of the outdoor temperature. The paired values are provided in Table 1.

Table 1: Parameters used to describe the HVAC system

Parameter	*Cooling coil efficiency* η	*COP*	T_{Ext}
Value	0.9	[4 : 2]	[20 : 40]

The variation of the COP over the whole period studied here is represented in Figure 8 as a Matlab boxplot. The first value on the abscissa corresponds to values obtained between midnight and 1 a.m. Since solar time is used, we recall that the occupancy period starts at 6 a.m. and ends at 4 p.m. The central mark within the boxes represents the median value and the edges of the box are the 25th and 75th percentile. The whiskers extend to the most extreme data points and the outliers are plotted individually.

These results clearly show a fall of the COP during the warmer daytime period and an increase during the night – until a maximum value is reached in the early morning. This prompts the search for an energy saving strategy, in which the system would store energy and release it later, thanks to its high thermal inertia. In other words, a ventilated slab could take advantage of the higher COP values to aim for energy savings. It is acknowledged that the estimation of the COP values is rough

compared to what can be observed on real devices. However, the main objective of this approach is to determine the potential of this energy saving strategy rather than to assess a precise value.

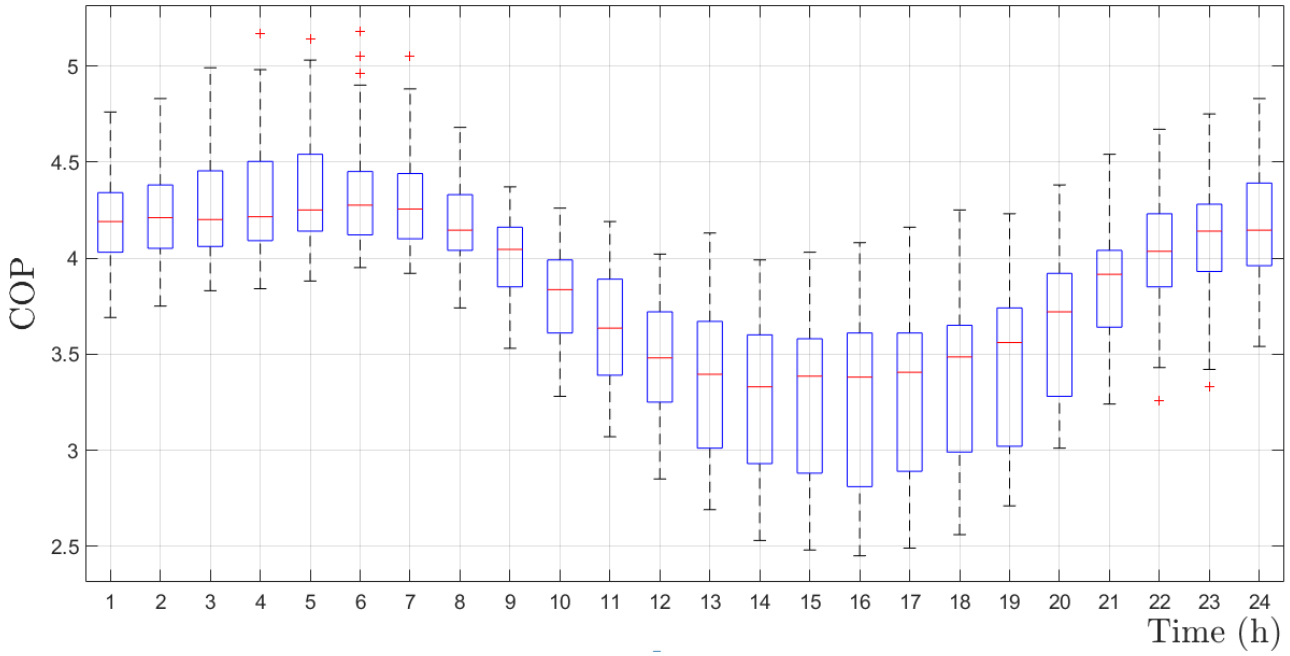

Figure 8 : Boxplot of the COP values over the 30-day long period.

In practice, an HVAC system has local control loops that control the air temperature at the output of the cooling and heating sections, the flow rate provided by the fans, etc. In this study, the dynamics associated to these local loops were not modelled. Typical dynamics of these local loops is much faster compared to the dynamics of the TABS and the building. Thus, at the perspective of the building/TABS dynamics, the local control loops are considered as being ideal controllers ensuring zero static error. The manipulated variables by these local controllers are the water temperature that enters the cooling coil and the power supply to the heating coil. These information enables to compute the amount of energy that is consumed by the HVAC. Nevertheless, this input temperature of the water is bounded by upper/lower limits which are physically achievable (i.e. minimum temperature is the one supplied by the chiller and the maximum temperature is the one for water return from the coil). There is only a lower limit for the heating coil power, which is zero. The control of the mixing damper is however considered because it has an impact on the static performance. It is a three-position control law that is explained in Table 3.

2.5. Indoor moisture balance

As mentioned above, the cooling demand is influenced by the moisture content of the air, mostly because of condensation in the cooling coil. Since the outdoor and the indoor air are mixed prior to cooling, which gives r_M and T_M in equation (8), their moisture contents have to be determined in order to provide an accurate estimate of the energy required. While this calculation is straightforward for the outdoor air, this is not the case for the indoor air, which is reused. This paper proposes to rely on a moisture balance at room scale. It gives the pressure vapour of indoor air, which is included in the definition of the moisture content of air as follows:

$$r = \frac{R_{Da}}{R_v}\frac{p_v}{p_{atm} - p_v} \tag{10}$$

where R_{Da} and R_v are the specific gas constants for dry air and vapour respectively, p_{atm} is the atmospheric pressure and is supposed to remain constant (101325 Pa).

Moisture balance at room scale is influenced by the ventilation system, of course, but also by indoor sources and mass (water vapour) transfer with the room walls and furniture. For mass transfer with the walls and furniture, very fine approaches are required to define the mass flux precisely, such as exemplified in [26]. On the other hand, simplified approaches exist, such as the effective capacitance and the effective moisture penetration depth models. Based on these two approaches, [27] define the Hygric Inertia of the Room (HIR*) for a given moisture production scheme. This has the advantage of being based on experimental measurements in a real furnished room and allows fast calculation of the indoor moisture balance, which was proposed by the authors as:

$$\left(\frac{V_{Room}}{R_v T_{Room}} + \frac{100\ HIR^*\ V_{Room}}{p_{v,Sat}(T_{Room})}\right)\frac{\partial p_{V,Room}}{\partial t} = \frac{\dot{m}}{\rho_A R_v T_{Room}}\left(p_{v,in} - p_{v,Room}\right) + G_v \tag{11}$$

where p_v is the partial vapour pressure (Pa), R_v is the gas constant for water vapour (462 J.kg^{-1}.K^{-1}), HIR^* is the Hygric Inertia of the Room (kg.m^{-3}.% RH^{-1}), and G_v (kg.s^{-1}) is the indoor vapour source.

Experimental tests were conducted by [27] on a furnished student room of 35 m^3 and led to an HIR* value of 0.72 10^{-3} $kg.m^{-3}.\%RH^{-1}$ when water vapour was emitted continuously for 8 h every day. Since the schedule and inside dimensions used by [27] are similar to those of the office studied here, the same value was used in the present study as a first approximation. Indoor vapour sources were set constant during working hours (8 a.m. to 6 p.m.) and represented the mass flow rate of breathing for two persons (48 $g_v.h^{-1}$ per person, as in [26]).

All the equations presented in this chapter were implemented in the Simulink Environment, which meant that heat transfer within the slab, moist air properties at different positions of the HVAC system, and heat and mass balance at the room scale were all simulated together. The outputs of the model are the room temperature and moisture content as well as the power demand for the cooling and the heating coils. The inputs are the outdoor conditions, the schedule for the internal heat loads, and the temperature set point at the inlet of the ventilated slab (T_{in}).

3. Model Predictive Control (MPC)

The objective is to maintain the room temperature (T_{Room}) within the desired range. Since a constant airflow rate is provided to the ventilated slab, the objective of the controller is to define a suitable time series for the air temperature at the inlet of the slab (T_{in}). The first part of this section defines the temperature exceedance, which is the index used to represent the ability of the system to maintain the indoor temperature within the desired range. An important feature of the MPC is that it relies on an optimization technique, here a Genetic Algorithm. Both techniques are mature and this study does not intend to develop them. However, since their tuning remains a key feature as underlined by [14,28], it is presented in the appendices (section 8.3 and 8.4).

It is mandatory to define a temperature range for the indoor environment before defining the control system. The room temperature, among other parameters and phenomena (e.g. thermal radiation,

draughts, noise and clothing), strongly affects the occupants' comfort. For this reason, it is a very sensitive parameter that is often considered when seeking to achieve a trade-off between comfort and energy demand, as exemplified in [29]. In most private office buildings, however, the indoor temperature set-point remains within a narrow range [30]. Since this study does not intend to focus on the evaluation of comfort, it was decided to select a classical indoor temperature range that complies with current practice in private offices. For this reason, the targeted room temperature ranged between 21 and 25°C during working hours (from 8 a.m. to 6 p.m.). Outside this time, the room temperature was allowed to vary over a much larger range (from 15 to 30°C), to facilitate the use of the ventilated slab's thermal inertia.

The ability of the system to maintain the desired indoor temperature was estimated by computing the temperature exceedance, θ, defined as follows:

$$\theta = \int_0^t \max\left(T_{Room}(t) - T_{Up}(t); 0\right) + \max(T_{Low}(t) - T_{Room}(t); 0)\ dt \qquad (12)$$

where T_{Up} and T_{Low} are the upper and lower thresholds of the desired indoor temperature range.

θ is given in °C.h and takes both the duration and magnitude of the exceedance into account. Its definition allows negative and positive exceedances to be cumulated. An illustration is provided in Figure 9 for a fictitious indoor temperature evolution, but with the actual temperature thresholds.

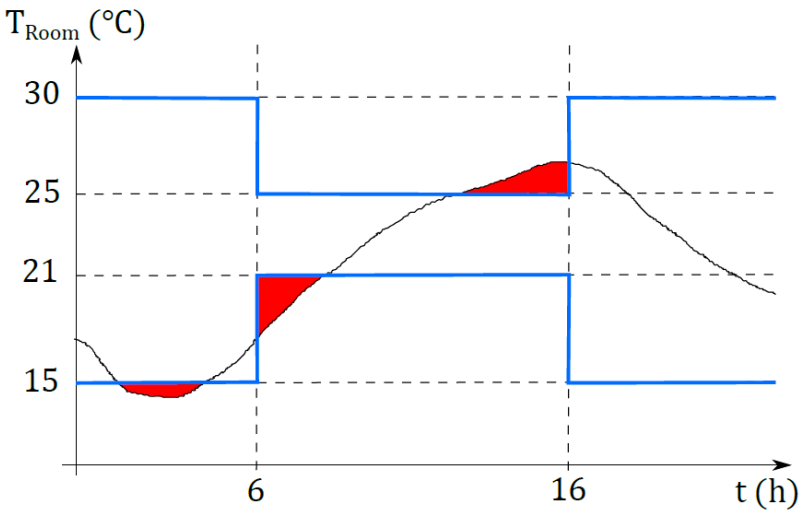

Figure 9 : Temperature thresholds T_{Up} and T_{Low} (thick blue lines), room temperature (black curve) and periods that account for the calculation of temperature exceedance θ (red surface).

The objective for the algorithm was to minimize the cost function *f*, which takes both the temperature exceedance and the energy demand into account. Penalty coefficients α were added in order to stress the influence of one of the two objectives as follows.

$$f = \alpha_E \, E + \alpha_\theta \, \theta \tag{13}$$

While energy demand does matter and drives a lot of research effort, energy savings are obtained at the cost of larger indoor temperature variations. In modern offices, however, people are used to experiencing a narrow temperature range and indoor temperature remains a key parameter in technical specifications. As one of the objectives was to demonstrate the ability of the ventilated slab to meet these specifications, it was decided to favour temperature exceedance in this study by using a high value for its penalty coefficient ($\alpha_\theta = 3$) while no penalty was applied to the energy demand ($\alpha_E = 1$). Such penalties led the algorithm to avoid temperature exceedance at all costs, so that maintaining the desired indoor temperature can be seen as a constraint more than an objective.

4. Results and discussion

This section presents a comparison of the different solutions proposed for maintaining the room temperature within the desired range. Firstly, the results obtained with a ventilated slab at 6 ACH will be analysed in detail for a 30-day period in order to provide insights into its behaviour. This case will stand as the reference case later in the paper. Second, the results obtained with this reference case will be set against the ones obtained with the regular (non-ventilated) slab. Finally, the influence of the mass flow rate will be studied by repeating the simulations for four other air change rates (instead of 6 ACH as in the reference case) and for the two types of slab.

4.1. Thermal behaviour of the room equipped with the ventilated slab

The room temperature obtained during the 30-day period is plotted as a boxplot diagram in Figure 10.

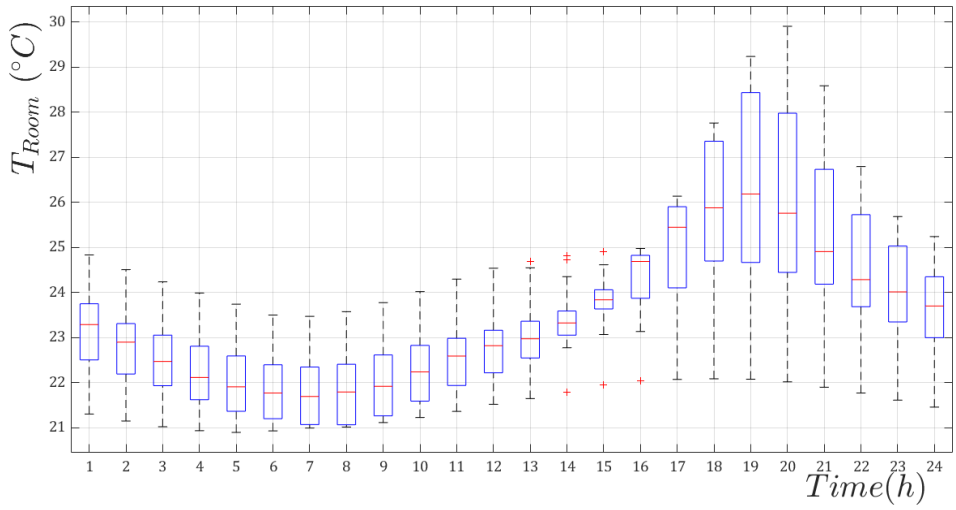

Figure 10: Room temperature distribution over the 30-day period (6 ACH, VS).

It can be seen that the room temperature remains within the desired range ([21: 25] °C) during occupancy (from 6 a.m. to 4 p.m., the reference used in the simulation being the solar hour). On the other hand, significantly higher temperatures are obtained at the end of the occupancy period, and values higher than 25 °C can be experienced up to midnight, although they remain below T_{up} (see Figure 9). The computed value of the temperature exceedance θ is lower than 1 °C.h for the whole period, meaning that the main objective, providing adequate room temperature, can be reached. Finally, it can be observed that T_{room} does not vary significantly in the early morning; in fact, it remains in the temperature range defined for occupancy for almost all the time, even if a larger temperature range is authorized. This means that there is no benefit to be derived from subcooling the room during the night. Figure 11 shows more details, with T_{room}, T_{in} and T_{ext} plotted against time for three consecutive hot days.

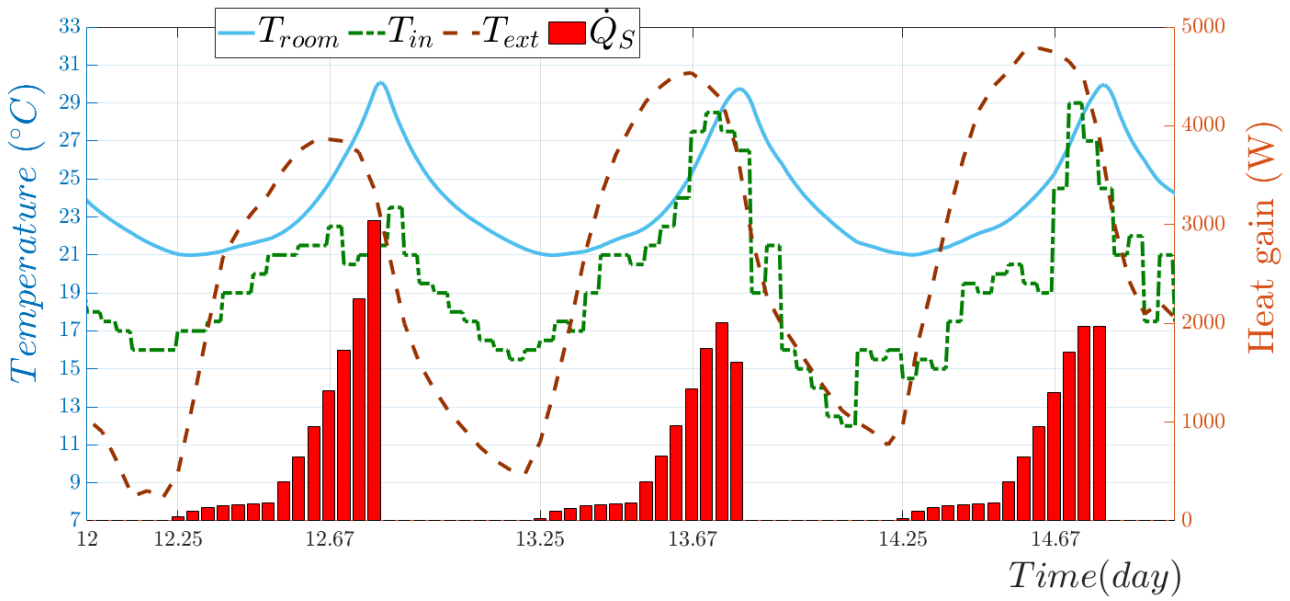

Figure 11: Room, inlet, outdoor temperature and solar heat gain during three hot days (x-scale was defined to meet the limits of the occupation period).

Although the daily magnitude of the outdoor temperature exceeds 20 °C, the room temperature remains within a narrower range and follows the same trend during the three days. T_{room} follows a slope that increases progressively during the day and reaches its maximum around 6 p.m. (solar time), then decreases rapidly to reach 21 °C just before the beginning of the next occupation period. The inlet temperature, T_{in}, is also similar during the three days. During occupation, the air enters the ventilated slab at a temperature that is equal to or lower than the room temperature, meaning that cooling has to be provided. Outside the occupation period, T_{in} is often set between the room and the outdoor temperature. Since the algorithm was designed to select a temperature with a 0.5 °C resolution that is constant for 1 hour, the values of T_{in} do not exactly respect the measured values of T_{room} and T_{ext}. But they show that comfortable indoor conditions can be obtained during occupancy by preferring free-cooling to mechanical cooling during the night for this period. This control strategy is able to maintain indoor temperature within the desired range and also favours low energy demand. However, it can be observed that the outdoor conditions favour free cooling since the outdoor temperature drops quickly during the night and reaches 10 °C. While the climatic conditions are those of Montpellier, which is very close to the Mediterranean Sea, these three hot days are not

representative of a heat wave where the control of the system is bound to be significantly different. In other words, the authors acknowledge that the results presented here are partial because the outdoor conditions remained mild compared to what has been experienced recently. To analyse the energy demand in more detail, the energy required for cooling is plotted in Figure 12 by means of a boxplot diagram.

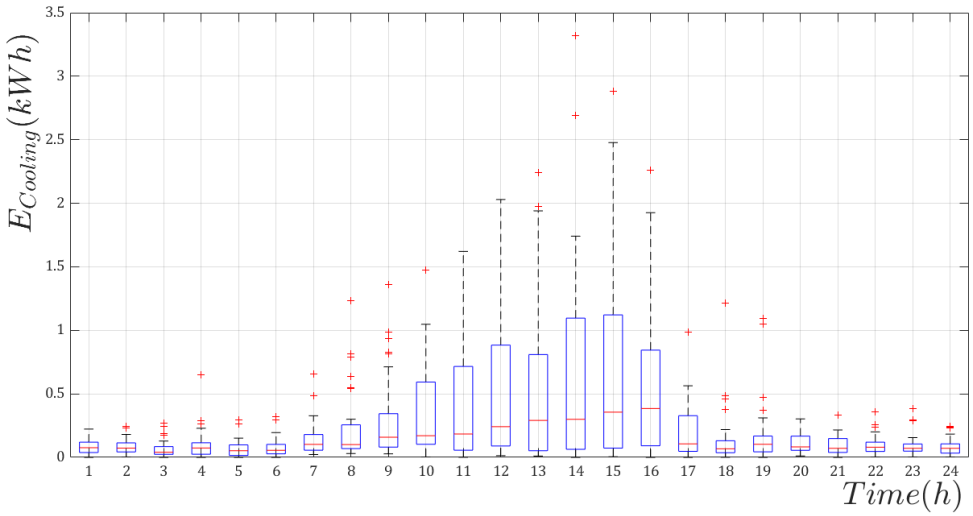

Figure 12: Energy demand for cooling over the 30-day period (6 ACH, VS).

First, it should be underlined that 96 % of the energy used during this period was for cooling, meaning that the heating demand was negligible. Second, it appears that the energy demand was very low outside the occupancy period: the magnitude of the hourly median value was 0.1 kWh and the highest value did not exceed 0.5 kWh. On the other hand, the energy demand rose progressively during the day and the maximum values were obtained during the afternoon. While the magnitude of the median values remained low, the variability of the energy demand was significantly higher: it often exceeded 0.5 kWh and could even be higher than 2 kWh punctually. This variability is representative of the diversity of the heat loads, especially when solar loads are considered (see Figure 5). Also, it is interesting to observe that, despite advantageous COP values during the night (see Figure 8), the optimized solution does not lie in cooling the ventilated slab to a very low temperature during the night. Instead, the cooling demand occurs when the heat loads are the highest and the COP is the lowest. Therefore, it can be said that, for the conditions of the test presented here,

the thermal inertia brought by the ventilated slab does not result the energy demand for cooling being shifted to the night period.

Finally, some parameters of lesser importance can be discussed. Indoor vapour pressure and temperatures were used to compute the indoor relative humidity. First, it was checked that the relative humidity remained lower than 1 throughout the period, ensuring consistency. Second, indoor humidity is hardly controlled in offices. In the present study, this resulted in strong variability over the whole period. The mean value was close to 55 % during occupancy, which is acceptable, but values higher than 80% were observed punctually and represent a total of 4 % of the occupancy period. The behaviour of the airflow mixer can be a key parameter in controlling indoor humidity and its control law could be improved to limit the occurrence of high values of relative humidity.

We recall that, in this study, as presented in section 8.2, only three options exist depending on the values of T_{in}, T_{Room} and T_{Ext}. The results were broken down and presented in Figure 13 in order to determine the probability of obtaining an option at a given time. The use of fresh air only ($\tau_1 = 1$) was slightly favoured (43 %) over the other two options (approximately 28.5 % for a mixture of indoor and fresh air, or the highest possible fraction of indoor air), but no clear trend appears. Overall, it can be concluded that basing the management of the airflow mixer on temperature and energy constraints alone does not lead to uncomfortable indoor conditions. In addition, using a fresh air fraction that is often significantly higher than the minimum should favour the removal of indoor pollutants and improve indoor air quality, generally speaking.

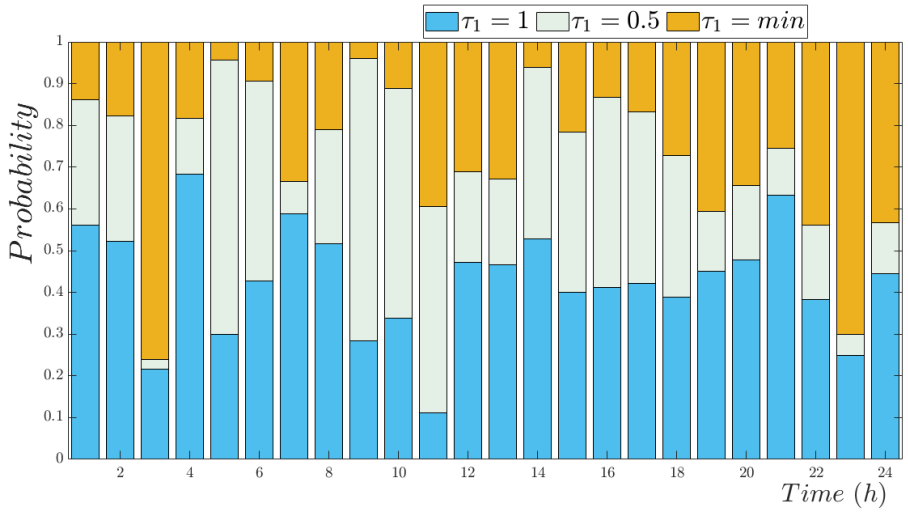

Figure 13: Probability of obtaining a given fraction of fresh (outdoor) air at the outlet of the air mixer over the 30-day period (6 ACH, VS)

4.2. Thermal behaviour of the room with a non-ventilated slab

The results obtained with a regular slab instead of the ventilated slab are analysed here. The boundary conditions remained exactly the same, as did the control algorithm. First, the temperatures obtained during the three hot days are presented in Figure 14, for the same period as for Figure 11.

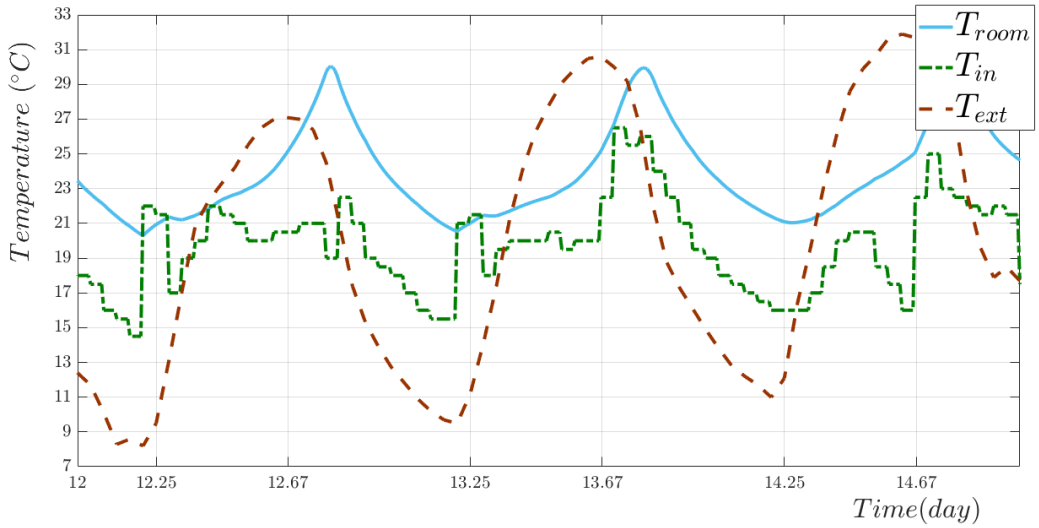

Figure 14: Room, inlet and outdoor temperature during three hot days (6 ACH, NVS)

First of all, the indoor temperature behaviour is very similar to what was observed with the ventilated slab. Smooth variations are observed despite the fact the regular slab provides less active thermal inertia and, although higher temperatures are experienced after occupancy, they remain below the upper threshold. The inlet temperature (T_{in}) is also similar during the first two days, but it differs

more significantly during the third day. For the VS, during the third day, the air handling unit had to prepare cooler air, by blowing only fresh air during the night (that is, using free cooling) or by turning on the cooling coil during the day, especially in the morning. This highlights the difference in terms of thermal behaviour between the two systems more significantly. To better analyse their difference, the inlet temperature and the room temperature obtained during the 30-day period are compared in Figure 15.

a)

b)

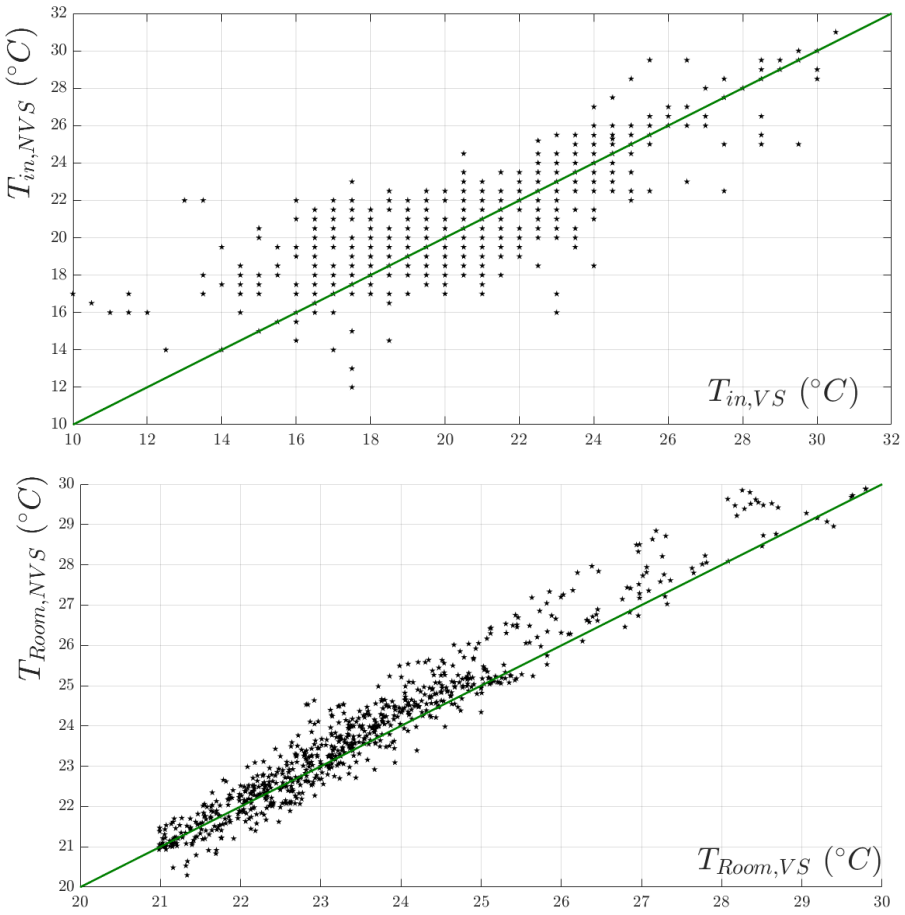

Figure 15: Comparison of T_{in} (a) and T_{room} (b) obtained for the VS (x axis) and the NVS (y axis). The thick line represents a perfect match.

These plots confirm that the inlet temperature varies more than the room temperature since the dots are more scattered in the former case. Also, it can be observed that the room temperature obtained with the NVS was slightly higher than with the ventilated slab. On the other hand, this was not so evident for the inlet temperature.

This qualitative comparison can be enriched by a quantitative indicator – the Pearson correlation coefficient (or linear correlation coefficient). Its definition relies on the covariance (denoted *cov*) between two variables (X and Y) normalized by the product of the standard deviations (σ), such that:

$$\rho_P(X,Y) = \frac{cov(X,Y)}{\sigma_X \, \sigma_Y} \tag{14}$$

The calculated values for T_{room} and T_{in} are 0.98 and 0.86 respectively, which strengthens the idea that, depending on the type of slab, the HVAC system has to behave differently to obtain similar room temperatures. This behaviour can now be analysed by comparing the energy demand in the two cases (see Figure 12 and Figure 16).

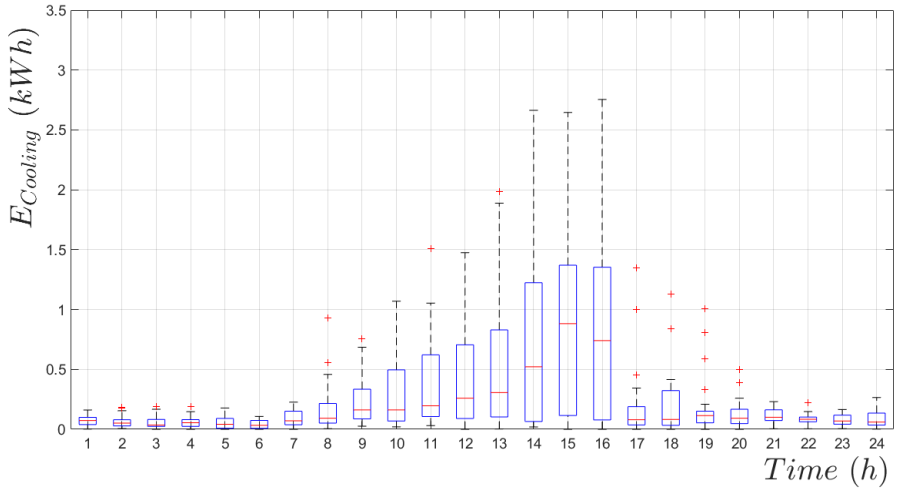

Figure 16: Energy demand for cooling (6 ACH, NVS).

Overall, both figures exhibit the same trend. If we focus on median values, however, the increase in the energy demand during the afternoon is more pronounced for the NVS than for the VS. Also, for the NVS system, the maximum hourly energy demand is slightly higher than for VS, which implies a higher power demand and consequently requires a larger HVAC system. Nevertheless, the energy demand is similar, since the difference is only + 6 % for the NVS.

This comparison between the two systems leads to the conclusion that a ventilated slab can perform as well as a regular (non-ventilated) slab, at least for the test cases presented here. This is consistent with the results obtained during an earlier study with a much more basic control law, namely a fixed

temperature set point combined with hysteresis for turning on the cooling coil [12]. However, it was also highlighted that the differences could become more significant at different airflow rates. Since 6 ACH is already a high value for airflow rates in offices, this comparison is extended to lower airflow rates in the next section.

4.3. On the influence of the mass flow rate

The computational work was repeated for the other 5 values of the air change rate, for the ventilated and the non-ventilated slab. For each configuration, the simulation was run 3 times in order to make sure that the stochastic method used in GA was correctly tuned and led to similar results. The results are presented in Table 2, which shows the total energy demand for heating and cooling, E, the temperature exceedance, θ, and the fraction of the energy used for cooling and dehumidifying.

Table 2 : Comparison of the energy performance levels obtained for different air change rates (mean value for 3 runs ± standard deviation)

Air change rate	System	E (kWh)	$\frac{E_{Cooling}}{E}$ (%)	$\frac{E_{Latent}}{E}$ (%)	θ (°C.h)
6 ACH	VS	36.3 ± 0.3	96.8 ± 0.5	13.5 ± 0.1	0.54 ± 0.03
	NVS	39.3 ± 0.2	93.2 ± 0.4	14.4 ± 0.2	0.14 ± 0.01
5 ACH	VS	39.0 ± 0.1	99.1 ± 0.1	16.0 ± 0.3	0.66 ± 0.01
	NVS	40.8 ± 0.4	95.8 ± 0.4	17.5 ± 0.1	0.15 ± 0.01
4 ACH	VS	44.1 ± 0.3	99.6 ± 0.1	18.5 ±0.3	0.76 ± 0.04
	NVS	43.1 ± 0.4	99.1 ± 0.1	21.5 ± 0.1	0.15 ± 0.01
3 ACH	VS	53.5 ± 0.2	99.8 ± 0.1	23.9 ±0.2	1.60 ± 0.06
	NVS	49.2 ± 0.4	99.8 ± 0.1	26.2 ± 0.2	0.51 ± 0.02
2 ACH	VS	70.8 ± 0.2	99.9 ± 0.1	35.6 ± 0.2	7.76 ± 0.16
	NVS	63.6 ± 0.3	99.9 ± 0.1	34.3 ± 0.2	6.07 ± 0.09

It appears that decreasing the air change rate has a similar effect on both systems. Overall, both the energy demand and the temperature exceedance increase. The influence is slight at first, when the air change rate diminishes to 5 or 4 ACH, especially if we focus on the temperature exceedance. For 3 and 2 ACH however, θ becomes significantly higher (> 1 °C.h^{-1}). The acceptability of such a value of temperature exceedance to the occupants can be debated. Nevertheless, the comparison reflects

the fact that the systems are less effective in controlling the indoor temperature at lower air change rates.

Regarding the energy demand, an interesting result is that more energy is used for dehumidifying the air at low air change rates: while the latent loads represent roughly 5 kWh at 6 ACH, they reach 23 kWh at 2 ACH, which is approximately 4.5 times more. The main reason for this is that providing the same cooling power at a lower mass flow rate necessarily implies that the temperature of the chilled water in the cooling coil, T_{wa}, has to be lowered. This can be clearly seen in Figure 17, where the temperature at the inlet of slab is very often set at the minimum (10 °C) at 2 ACH while this is never the case at 6 ACH (see Figure 11). The consequence is that the set point temperature is more often lower than the dew point temperature of the air entering the cooling coil. As a result, more air needs to be dehumidified and this comes at the cost of higher energy demand.

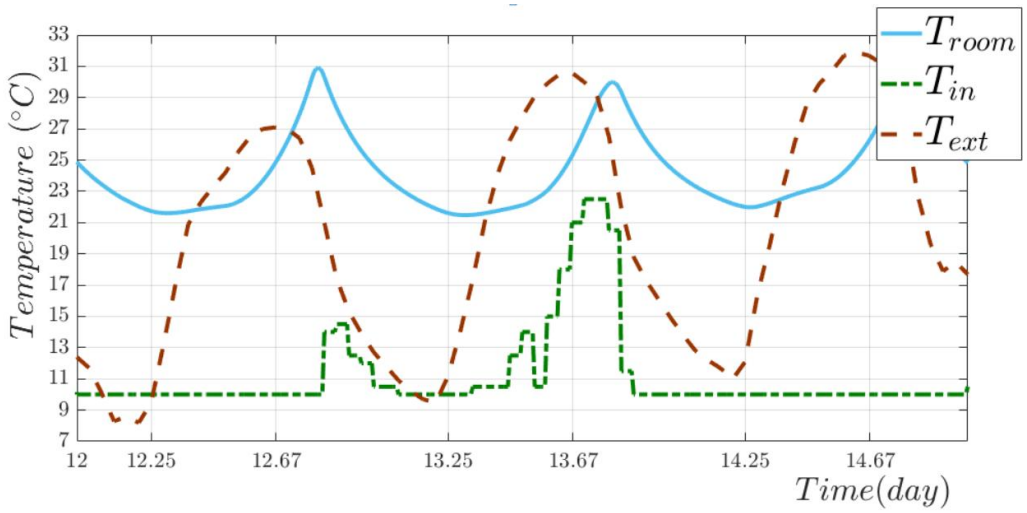

Figure 17: Room, inlet, and outdoor temperature during three hot days (2 ACH, VS).

Besides the change in the temperature set point for the air prepared within the HVAC system, it is interesting to look at the dynamics of the energy used for cooling. It is illustrated in Figure 18 for a minimum air change rate and for the case of a VS. Note that a very similar trend was obtained for an NVS but is not presented here for the sake of clarity. While a scattered distribution is observed at 6 ACH (see Figure 12), the trend is smoothed at 2 ACH: the median value is higher at 2 ACH but extreme values remain in a narrower range. This is a consequence of the smaller cooling power

available at 2 ACH. Finally, the maximum energy demand for cooling still occurs during occupancy, but it remains significant between 7 p.m. and 8 a.m., while it was negligible at this time for 6 ACH. The results presented in Figure 12 and Figure 18 show that, whatever the value of the air change rate, the strategy of focusing on the thermal inertia of the ventilated slab during the night to take advantage of higher COP values was not selected by the control algorithm. In other words, this strategy does not lead to the lowest energy demand. A different conclusion was obtained in [11], where the objective was to minimize the operation cost and when a significant ratio of on-peak to off-peak charges was used, highlighting the potential economic benefits of VS. When the ratio equals one however, meaning that operational cost does not depend on the period of the day, the conclusions of [11] are consistent with the results of the present paper.

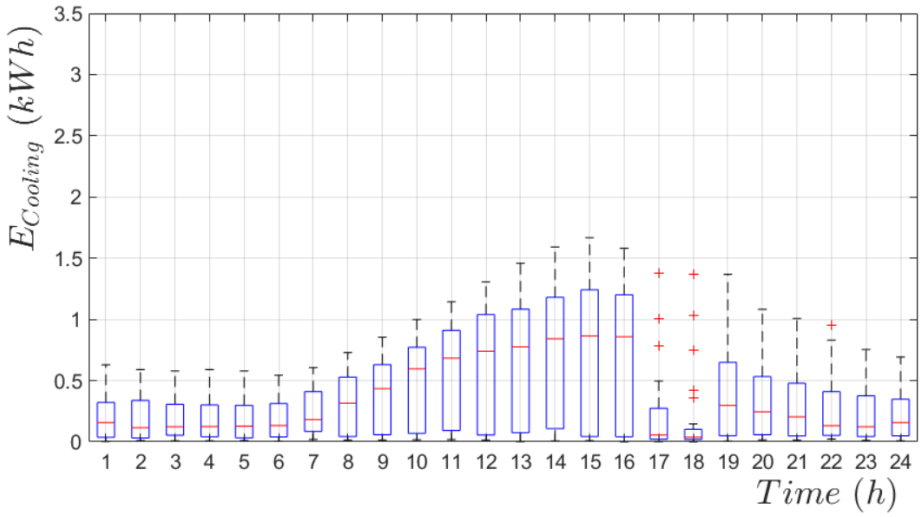

Figure 18: Energy required for cooling over the 30-day period (2 ACH, VS)

To further analyse the results, it is interesting to observe that reducing the airflow rate also has some positive impacts, since it reduces the energy demand of the fan, E_{Fan}, which was not considered until now. A rough estimation can be obtained with the following equation (used in NF EN 13779, 2009) for sizing a ventilation system.

$$E_{Fan} = SFP\ Q_V\ t \quad (15)$$

where *SFP* is the Specific Fan Power (kW.(m^3.s^{-1})$^{-1}$) and Q_v is the volumetric flow rate (m^3.s^{-1}).

It could be objected that the power of the fan is generally estimated as a cubic function of the volumetric flow rather than linear function, as proposed in [9]. This is the case for a given pipe network. But since a constant airflow rate should be used with this ventilated slab and since this study is focused on the design of the system and its control, it is foreseen that the pipe network would be adjusted to the retained value of the volumetric flow rate. Consequently, a linear trend is justified at the design stage under the assumption of constant airflow rate.

According to the examples provided in the standard, the magnitude of *SFP* values for Air Handling Units equipped with both air supply and extraction units lies around 2.5, which is the value chosen in the present study. Consequently, the energy demand for ventilation is sizeable for this test case: it reaches 150 kWh for 6 ACH, i.e. 4 times the energy demand for heating and cooling. The trade-off between the energy used for cooling and for ventilation for different air change rates is illustrated by Figure 19.

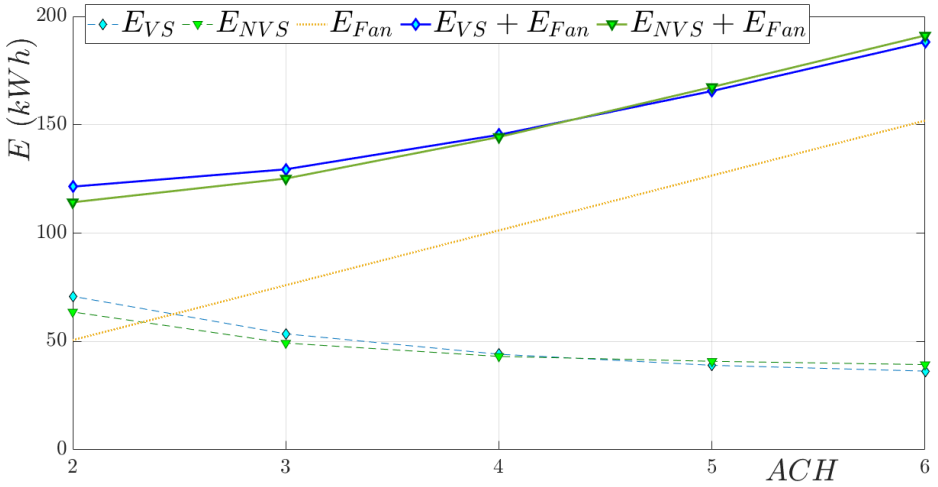

Figure 19: Estimation of the total energy demand (Heating, Cooling and Ventilation) according to the air change rate.

It is clear from Figure 19 that high air change rates should be avoided since the total energy demand increases dramatically. This is in line with the early conclusions of [9], which were obtained under simplified boundary conditions and no MPC. For low air change rates (2 and 3 ACH), the energy demands for cooling and ventilating are of the same magnitude. Since it has already been observed that the temperature exceedance rises significantly at 2 ACH, an air change rate of 3 ACH offers a

good compromise: the temperature exceedance remains acceptable compared to 2 ACH (see Table 2) at the cost of a slight increase in the total energy demand (+ 7 %).

Changing the air change rate also has an impact on the temperature at the outlet of the HVAC system T_{in}, as illustrated above. Despite the fact that a low threshold was defined for T_{in} (10 °C), such a marked temperature difference with room temperature can result in discomfort because the occupants may experience an ankle to head temperature difference. It is commonly accepted that such a difference affects thermal comfort negatively [32]. It is likely to happen with the displacement ventilation technique for example, which consists of blowing cold air close to the floor at low velocities. Such a situation is very likely to occur when buoyancy forces become more significant, i.e. when the temperature difference between the supply air and the room is the greatest. This situation can be managed by means of a detailed Computational Fluid Dynamics (CFD) study to optimize air distribution strategy, as exemplified in [33], by multiplying the number of supply air terminals for example. One strong advantage of the ventilated slab is that the temperature of the air blown into the room, T_B, is different from T_{in} because of the heat transfer within the slab. This behaviour is illustrated in Figure 20 for four different cases. Generally speaking, the temperature difference obtained with ventilated slabs is lower than with a regular slab. This difference is slight at 6 ACH and should not have a significant influence on comfort since the temperature difference remains small (> -8°C) most of the time. When the air change rate decreases to 3 ACH, however, the results reveal substantial differences. Both distributions are shifted to the left, meaning that the temperature difference is increased, but the one for the NVS is spread over a much wider range, down to -15 °C in extreme situations (in the late afternoon of hot days). From these results, it can be assumed that the ventilated slab should provide more comfortable indoor conditions at lower air change rates. However, more work is required to strengthen this statement, for example, by carrying out 3D CFD studies within the room.

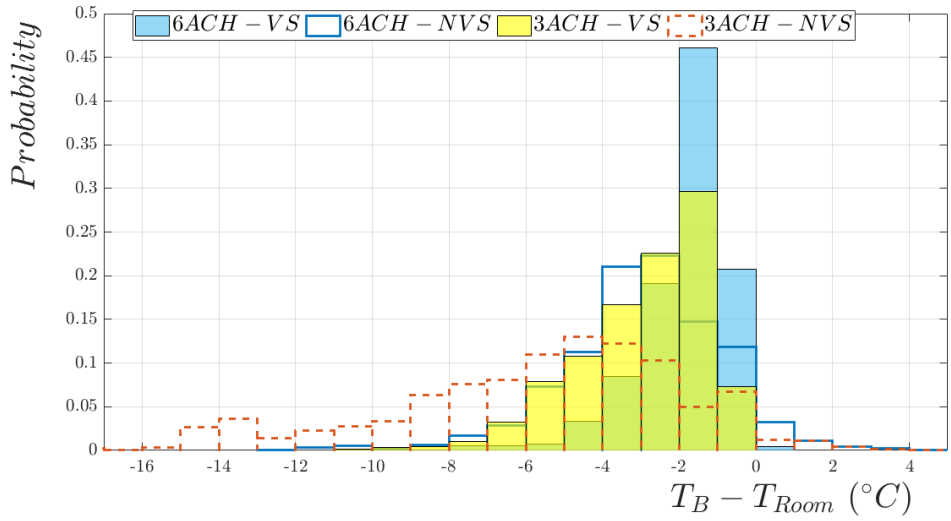

Figure 20: Distribution of the temperature difference between the air blown into the room and the ambient air for 4 cases.

4.4. Discussion

The results presented in this study are promising in the framework of the development of the ventilated slab. They were in line with some of the results obtained in [9,11], increasing the number of published case studies dealing with ventilated slabs. However, much remains to be done before they can be used with confidence in real buildings.

First of all, it has been underlined above that the boundary conditions used here favoured free cooling and made a subcooling strategy unnecessary. However, harsher conditions are bound to arise in the coming years, during heatwaves for example. The pros and cons of the ventilated slab should be analysed in greater depth and thus explore a wider range of situations. The encouraging results obtained here motivate the use of finer models of the building elements, outdoor conditions and HVAC elements. It is foreseen that another modelling environment than Matlab would suit better such a purpose.

Another limitation of the present work is that the predictive controller remains an offline/simulation application. Its integration into a Building Automation System (BAS) remains challenging according to [34], largely because of the computational time necessary for MPC. This issue could be overcome

with rule extraction techniques that could be more easily implemented in a BAS, for example. However, this method is not straightforward and requires more efforts. The second limitation of offline techniques is that all the heat loads are perfectly known for the receding horizon (or the time span window) when the optimization is run but the real heat loads might differ: because of uncertainties in weather forecasting, unexpected use of appliances and the stochastic nature of occupancy. This mismatch between the values used for performing optimization and the actual values can impact the optimality of the solutions and possibly lead to uncomfortable indoor conditions. In the specific context of offices, this risk matters because it strongly influences the occupants' opinions on the reliability of ventilated slabs, while the energy demand is often regarded as of minor importance. It is therefore necessary to address the robustness of MPC for ventilated slabs. This is a rather classical issue with MPC, but the techniques used to deal with it may differ significantly. A technique involving low computational cost was proposed in [35] to determine the optimal chilled loading under uncertain cooling demand. Huang and Sun (2019) used a stochastic process (Monte Carlo) to better assess the control signal for a cluster of electric batteries when the thermal properties of the building were uncertain. On the other hand, the uncertainties have been modelled as a polytope and the optimization problem reformulated using linear matrix inequalities [37]. Assessing robustness is a broad topic that would also require a significant effort.

In addition to advanced control and modelling techniques, the possibility of moving from a constant airflow to a variable airflow should be explored. As highlighted earlier, the differences between a ventilated slab and a regular slab become less pronounced for higher airflow rates, because a significantly higher fraction of the heat flux is blown directly into the room and not delayed by the thermal inertia of the slab. This means that increasing the airflow rate would allow mismatches to be easily dealt with, since it would provide a fast response to indoor temperature drifts, reducing the risk of significant temperature exceedance. This can be easily implemented on real devices. On the other

hand, the theoretical study of a variable airflow system raises the issue of modelling nonlinear heat transfer in the ventilated slab, since this is not possible with classical techniques for model reduction.

5. Conclusions

This paper proposes a relative comparison of the energy demand and indoor temperature obtained with a ventilated slab and a regular (non-ventilated) slab. The results indicate that the indoor temperature was maintained within the desired range most of the time with no significant difference between the two systems, although higher discrepancies appeared for the lowest airflow rate (2 ACH). The differences in terms of energy demand were also minor between the two systems, but a lower airflow rate was preferable as it decreased the electricity consumption of the fans, which was significant for this test case. In fact, the most important difference lies in the temperature difference between the air blown into the room and the air already in the room: the difference is significantly lower for ventilated slabs at low airflow rates, suggesting that ventilated slabs should provide more comfortable indoor conditions. Beyond that, this study shows that ventilated slabs should perform as well as a more classical system when combined with an MPC, for the case study presented here. A finer modelling of the building and HVAC system should be considered to strengthen this statement, so as a wider range of boundary conditions.

Further research should deal with the ability of MPCs to tackle uncertainties in the prediction of the heat loads and outdoor temperature. Unlike other TABS, a ventilated slab can easily handle such a situation by simply increasing the airflow rate punctually. Actually, its behaviour approaches that of a regular slab as the airflow increases, meaning that the thermal inertia is bypassed and the cooling power is brought directly to the room. However, modelling a variable air flow rate system with high thermal inertia is challenging and will require more efforts.

6. References

[1] M. Isaac, D.P. van Vuuren, Modeling global residential sector energy demand for heating and air conditioning in the context of climate change, Energy Policy. 37 (2009) 507–521. https://doi.org/10.1016/j.enpol.2008.09.051.

[2] H. Alkhatib, P. Lemarchand, B. Norton, D.T.J. O'Sullivan, Deployment and control of adaptive building facades for energy generation, thermal insulation, ventilation and daylighting: A review, Appl. Therm. Eng. 185 (2021) 116331. https://doi.org/10.1016/j.applthermaleng.2020.116331.

[3] P.M. Congedo, C. Baglivo, D. D'Agostino, I. Zacà, Cost-optimal design for nearly zero energy office buildings located in warm climates, Energy. 91 (2015) 967–982. https://doi.org/10.1016/j.energy.2015.08.078.

[4] T. Kuczyński, A. Staszczuk, M. Gortych, R. Stryjski, Effect of thermal mass, night ventilation and window shading on summer thermal comfort of buildings in a temperate climate, Build. Environ. 204 (2021) 108126. https://doi.org/10.1016/j.buildenv.2021.108126.

[5] P. Blondeau, M. Spérandio, F. Allard, Night ventilation for building cooling in summer, Sol. Energy. 61 (1997) 327–335. https://doi.org/10.1016/S0038-092X(97)00076-5.

[6] C. Kendrick, R. Ogden, X. Wang, B. Baiche, Thermal mass in new build UK housing: A comparison of structural systems in a future weather scenario, Energy Build. 48 (2012) 40–49. https://doi.org/10.1016/j.enbuild.2012.01.009.

[7] J. Romaní, A. de Gracia, L.F. Cabeza, Simulation and control of thermally activated building systems (TABS), Energy Build. 127 (2016) 22–42. https://doi.org/10.1016/j.enbuild.2016.05.057.

[8] K.-N. Rhee, B.W. Olesen, K.W. Kim, Ten questions about radiant heating and cooling systems, Build. Environ. 112 (2017) 367–381. https://doi.org/10.1016/j.buildenv.2016.11.030.

[9] R. Winwood, R. Benstead, R. Edwards, Advanced fabric energy storage II: Computational fluid dynamics modelling, Build. Serv. Eng. Res. Technol. 18 (1997) 7–16. https://doi.org/10.1177/014362449701800102.

[10] R. Zmeureanu, P. Fazio, Thermal performance of a hollow core concrete floor system for passive cooling, Build. Environ. 23 (1988) 243–252. https://doi.org/10.1016/0360-1323(88)90009-1.

[11] B. Park, M. Krarti, Optimal control strategies for hollow core ventilated slab systems, J. Build. Eng. 24 (2019) 100762. https://doi.org/10.1016/j.jobe.2019.100762.

[12] M. Labat, I. Hazyuk, M. Cezard, S. Lorente, Indoor thermal behaviour of an office equipped with a ventilated slab: a numerical study, J. Build. Perform. Simul. 14 (2021) 227–246. https://doi.org/10.1080/19401493.2021.1905714.

[13] M. Sourbron, R. De Herdt, T. Van Reet, W. Van Passel, M. Baelmans, L. Helsen, Efficiently produced heat and cold is squandered by inappropriate control strategies: A case study, Energy Build. 41 (2009) 1091–1098. https://doi.org/10.1016/j.enbuild.2009.05.015.

[14] Y. Yao, D.K. Shekhar, State of the art review on model predictive control (MPC) in Heating Ventilation and Air-conditioning (HVAC) field, Build. Environ. 200 (2021) 107952. https://doi.org/10.1016/j.buildenv.2021.107952.

[15] Z. Jiang, P. Hlanze, J. Cai, Optimal predictive control of phase change material-based energy storage in buildings via mixed-integer convex programming, Appl. Therm. Eng. 215 (2022) 118821. https://doi.org/10.1016/j.applthermaleng.2022.118821.

[16] H. Viot, A. Sempey, L. Mora, J.C. Batsale, J. Malvestio, Model predictive control of a thermally activated building system to improve energy management of an experimental building: Part I—Modeling and measurements, Energy Build. 172 (2018) 94–103. https://doi.org/10.1016/j.enbuild.2018.04.055.

[17] M. Hu, F. Xiao, J.B. Jørgensen, R. Li, Price-responsive model predictive control of floor heating systems for demand response using building thermal mass, Appl. Therm. Eng. 153 (2019) 316–329. https://doi.org/10.1016/j.applthermaleng.2019.02.107.

[18] J. Vivian, L. Croci, A. Zarrella, Experimental tests on the performance of an economic model predictive control system in a lightweight building, Appl. Therm. Eng. 213 (2022) 118693. https://doi.org/10.1016/j.applthermaleng.2022.118693.

[19] I. Hazyuk, C. Ghiaus, D. Penhouet, Model Predictive Control of thermal comfort as a benchmark for controller performance, Autom. Constr. 43 (2014) 98–109. https://doi.org/10.1016/j.autcon.2014.03.016.

[20] J. (Dove) Feng, F. Chuang, F. Borrelli, F. Bauman, Model predictive control of radiant slab systems with evaporative cooling sources, Energy Build. 87 (2015) 199–210. https://doi.org/10.1016/j.enbuild.2014.11.037.

[21] A. Isanska-Cwiek, Experimental and CFD research on the thermal performance of the air cooled slab system, in: Montréal, Canada, 2005: pp. 443–450.

[22] K.J. Lomas, S. Oliveira, P. Warren, V.J. Haines, T. Chatterton, A. Beizaee, E. Prestwood, B. Gething, Do domestic heating controls save energy? A review of the evidence, Renew. Sustain. Energy Rev. 93 (2018) 52–75. https://doi.org/10.1016/j.rser.2018.05.002.

[23] H. Johra, P. Heiselberg, Influence of internal thermal mass on the indoor thermal dynamics and integration of phase change materials in furniture for building energy storage: A review, Renew. Sustain. Energy Rev. 69 (2017) 19–32. https://doi.org/10.1016/j.rser.2016.11.145.

[24] I. Hazyuk, C. Ghiaus, D. Penhouet, Optimal temperature control of intermittently heated buildings using Model Predictive Control: Part I – Building modeling, Build. Environ. 51 (2012) 379–387. https://doi.org/10.1016/j.buildenv.2011.11.009.

[25] A. Rodler, J. Virgone, J.-J. Roux, Adapted time step to the weather fluctuation on a three dimensional thermal transient numerical model with sun patch: Application to a low energy cell, Energy Build. 155 (2017) 238–248. https://doi.org/10.1016/j.enbuild.2017.09.027.

[26] R. Bui, M. Labat, S. Lorente, Impact of the occupancy scenario on the hygrothermal performance of a room, Build. Environ. 160 (2019) 106178. https://doi.org/10.1016/j.buildenv.2019.106178.

[27] E. Vereecken, S. Roels, H. Janssen, In situ determination of the moisture buffer potential of room enclosures, J. Build. Phys. 34 (2011) 223–246. https://doi.org/10.1177/1744259109358268.

[28] L. Gosselin, M. Tye-Gingras, F. Mathieu-Potvin, Review of utilization of genetic algorithms in heat transfer problems, Int. J. Heat Mass Transf. 52 (2009) 2169–2188. https://doi.org/10.1016/j.ijheatmasstransfer.2008.11.015.

[29] M. Lakeridou, M. Ucci, A. Marmot, I. Ridley, The potential of increasing cooling set-points in air-conditioned offices in the UK, Appl. Energy. 94 (2012) 338–348. https://doi.org/10.1016/j.apenergy.2012.01.064.

[30] A. Aryal, B. Becerik-Gerber, Energy consequences of Comfort-driven temperature setpoints in office buildings, Energy Build. 177 (2018) 33–46. https://doi.org/10.1016/j.enbuild.2018.08.013.

[31] NF EN 13779, Ventilation for non-residential buildings Performance requirements for ventilation and room-conditioning systems, (2009).

[32] B. Yang, A.K. Melikov, A. Kabanshi, C. Zhang, F.S. Bauman, G. Cao, H. Awbi, H. Wigö, J. Niu, K.W.D. Cheong, K.W. Tham, M. Sandberg, P.V. Nielsen, R. Kosonen, R. Yao, S. Kato, S.C. Sekhar, S. Schiavon, T. Karimipanah, X. Li, Z. Lin, A review of advanced air distribution methods - theory, practice, limitations and solutions, Energy Build. 202 (2019) 109359. https://doi.org/10.1016/j.enbuild.2019.109359.

[33] H. Yamasawa, T. Kobayashi, T. Yamanaka, N. Choi, M. Cehlin, A. Ameen, Effect of supply velocity and heat generation density on cooling and ventilation effectiveness in room with impinging jet ventilation system, Build. Environ. 205 (2021) 108299. https://doi.org/10.1016/j.buildenv.2021.108299.

[34] P.T. May-Ostendorp, G.P. Henze, B. Rajagopalan, D. Kalz, Experimental investigation of model predictive control-based rules for a radiantly cooled office, HVACR Res. 19 (2013) 15. https://doi.org/10.1080/10789669.2013.801303.

[35] M. Saeedi, M. Moradi, M. Hosseini, A. Emamifar, N. Ghadimi, Robust optimization based optimal chiller loading under cooling demand uncertainty, Appl. Therm. Eng. 148 (2019) 1081–1091. https://doi.org/10.1016/j.applthermaleng.2018.11.122.

[36] P. Huang, Y. Sun, A robust control of nZEBs for performance optimization at cluster level under demand prediction uncertainty, Renew. Energy. 134 (2019) 215–227. https://doi.org/10.1016/j.renene.2018.11.024.

[37] H. Nagpal, A. Staino, B. Basu, Robust model predictive control of HVAC systems with uncertainty in building parameters using linear matrix inequalities, Adv. Build. Energy Res. 14 (2020) 338–354. https://doi.org/10.1080/17512549.2019.1588165.

[38] E.P. del Barrio, An efficient method for solving large-scale differential sensitivity problems, Numer. Heat Transf. Part B Fundam. 43 (2003) 353–372. https://doi.org/10.1080/713836222.

[39] M. Labat, S. Lorente, M. Mosa, Influence of the arrangement of multiple radiant ceiling panels on the radiant temperature field, Int. J. Therm. Sci. 149 (2020) 106184. https://doi.org/10.1016/j.ijthermalsci.2019.106184.

[40] H.-G. Beyer, H.-P. Schwefel, Evolution strategies–A comprehensive introduction, Nat. Comput. 1 (2002) 3–52.

[41] J. Dreo, A. Petrowski, E. Taillard, Métaheuristiques pour l'optimisation difficile, EYROLLES, 2003.

7. Acknowledgments

The authors would like to thank IC Entreprises for supporting this research work and Guillaume Rabut for sharing his experience and expertise related to Vinci's GreenFloor® system.

8. Appendices

8.1. State space model of the regular slab

The slab is considered to exchange heat with the room by convection through its lower side only. All the other sides are assumed adiabatic. Such assumptions are consistent with a 1D transient heat problem that can be easily solved by means of a classic numerical approach. Here, the problem can be represented as an R-C network, as illustrated in Figure 21.

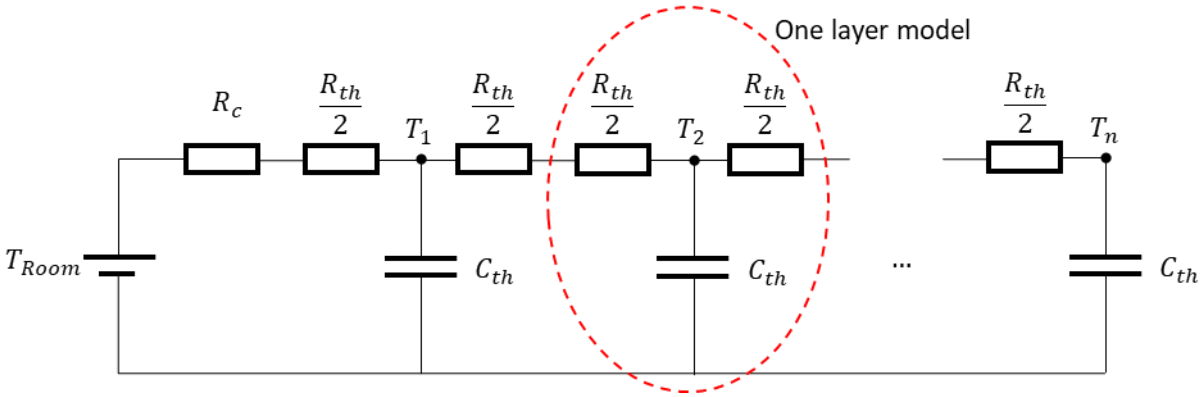

Figure 21 : Detailed 1D R-C model of a non-ventilated slab.

The slab, of thickness e and bottom surface area S, is split into n thin layers, each being characterized by its thermal resistance and thermal capacity given by:

$$R_{th} = \frac{e/n}{\lambda S}$$
$$C_{th} = \frac{e}{n} S \rho C_p \quad (16)$$

Each layer is represented by a capacity sandwiched between two halves of the resistance. Thus, the slab model is obtained by stacking n models of a single layer, where a different resistance R_c is applied to account for convective and radiative heat transfer. A typical value of $8\, W.m^{-2}.K^{-1}$ was selected in the present study. The equations that govern the dynamics of the temperature of each layer are:

$$
\begin{aligned}
C_{th}\frac{dT_1}{dt} &= \frac{1}{\frac{R_{th}}{2}+R_c}(T_{Room}-T_1)+\frac{1}{R_{th}}(T_2-T_1)\\
C_{th}\frac{dT_2}{dt} &= \frac{1}{R_{th}}(T_1-T_2)+\frac{1}{R_{th}}(T_3-T_2)\\
&\vdots\\
C_{th}\frac{dT_i}{dt} &= \frac{1}{R_{th}}(T_{i-1}-T_i)+\frac{1}{R_{th}}(T_{i+1}-T_i)\\
&\vdots\\
C_{th}\frac{dT_n}{dt} &= \frac{1}{R_{th}}(T_{n-1}-T_n)
\end{aligned}
\tag{17}
$$

The heat flux exchanged with the room at the lower face is, considering positive values of heat flux entering the slab:

$$
\dot{Q}_c = \frac{1}{R_{th}/2+R_c}(T_{Room}-T_1) \tag{18}
$$

This set of *n* equations can be modified to fit the state-space representation by using the following considerations:

- The state vector, x, expresses the temperature of each node, which corresponds to the temperature on the capacity of every layer ;
- The input of the system, u, is the room air temperature ;
- The output of the model, y, is the heat flux $\dot{Q}_c$.

$$
\begin{gathered}
x = [T_1 \quad T_2 \quad \cdots \quad T_i \quad \cdots \quad T_n]^{'}\\
u = T_{Room}\\
y = \dot{Q}_c
\end{gathered}
\tag{19}
$$

which gives the following state space matrices:

$$\boldsymbol{A} = \begin{bmatrix} -\frac{1}{C_{th}}\left(\frac{2}{R_{th}+2R_c}+\frac{1}{R_{th}}\right) & \frac{1}{R_{th}C_{th}} & 0 & \cdots & 0 \\ \vdots & & \vdots & & \vdots \\ 0 & \cdots & \frac{1}{R_{th}C_{th}} & -\frac{2}{R_{th}C_{th}} & \frac{1}{R_{th}C_{th}} & \cdots & 0 \\ \vdots & & \vdots & & \vdots \\ 0 & \cdots & 0 & \frac{1}{R_{th}C_{th}} & -\frac{1}{R_{th}C_{th}} \end{bmatrix} \quad (20)$$

$$B = \begin{bmatrix} \frac{2}{R_{th}C_{th}+2R_cC_{th}} \\ \vdots \\ 0 \\ \vdots \\ 0 \end{bmatrix},\ C = \begin{bmatrix} -\frac{2}{R_{th}+2R_c} & 0 & \dots & 0 \end{bmatrix},\ D = \begin{bmatrix} \frac{2}{R_{th}+2R_c} \end{bmatrix}$$

A large number of layers results in a dynamic model of a size that is prohibitive for control applications. A classical way to reduce large state-space models is to reproduce only the slower dynamics, the rapid ones being captured by the static part of the model [38]. Usually, the number of slow state variables is very small compared to the number of states in the detailed model.

The rapidity of the dynamics is given by the eigenvalues of the dynamic matrix A. The classical way to proceed with the model reduction is to first diagonalize the matrix A so that the eigenvalues appear on the main diagonal and group the slow and the fast dynamics as:

$$\begin{cases} \begin{bmatrix} \dot{x}_{slow} \\ \dot{x}_{fast} \end{bmatrix} = \begin{bmatrix} A_{slow} & 0 \\ 0 & A_{fast} \end{bmatrix} \begin{bmatrix} x_{slow} \\ x_{fast} \end{bmatrix} + \begin{bmatrix} B_{slow} \\ B_{fast} \end{bmatrix} u \\ y = \begin{bmatrix} C_{slow} & C_{fast} \end{bmatrix} \begin{bmatrix} x_{slow} \\ x_{fast} \end{bmatrix} + Du \end{cases} \quad (21)$$

Then, the derivatives of the fast state variables are cancelled ($\dot{x}_{fast} = 0$), which gives a new reduced state-space model:

$$\begin{cases} \dot{x}_{slow} = A_{slow}x_{slow} + B_{slow}u \\ y = C_{slow}x_{slow} + \left[D - C_{fast}A_{fast}^{-1}B_{fast}\right]u \end{cases} \quad (22)$$

As can be seen, the fast dynamics does not disappear; it just becomes part of the static model (the new feed-through matrix D).

8.2. Equations used for the airflow mixer

The temperature and moisture content at the outlet of the airflow mixer are given by:

$$T_M = \tau_1 T_{outdoor} + \tau_2 T_{room}$$
$$r_M = \tau_1 r_{outdoor} + \tau_2 r_{room} \quad (23)$$

where τ_1 and τ_2 are determined by considering the logic presented in Table 3. The idea is that a minimum amount of outdoor air $\dot{m}_{min}$ (equivalent to 1 ACH) has to be introduced permanently, but it might be profitable to re-use a given fraction of the indoor air. While it is theoretically possible to mix the two airflows to obtain any intermediate temperature at the outlet, this is hardly achievable in reality. For this reason, it was decided to select only 3 positions for the valve, depending on the temperatures T_{in}, T_{room} and T_{ext}.

Table 3 : Logic used for controlling the airflow mixer.

Condition	τ_1	τ_2
$T_{in} < T_{room} \leq T_{ext}$	$\frac{\dot{m}_{min}}{\dot{m}}$	$\frac{\dot{m} - \dot{m}_{min}}{\dot{m}}$
$T_{room} \leq T_{in} < T_{ext}$	$\frac{\dot{m}}{2}$	$\frac{\dot{m}}{2}$
$T_{in} \leq T_{ext} < T_{room}$	$\dot{m}$	0
$T_{ext} < T_{in} \leq T_{room}$	$\frac{\dot{m}}{2}$	$\frac{\dot{m}}{2}$
$T_{ext} \leq T_{room} < T_{in}$	$\frac{\dot{m}_{min}}{\dot{m}}$	$\frac{\dot{m} - \dot{m}_{min}}{\dot{m}}$
$T_{room} < T_{ext} \leq T_{in}$	$\dot{m}$	0

8.3. Genetic algorithm

The optimization process was undertaken by means of a Genetic Algorithm (GA), which is now accepted as a mature technique [28]. Although several algorithms are available, a custom algorithm,

developed previously in another framework [39], was adapted to the present study. Even though this demanded some programming efforts, it also offered the opportunity to tailor evolution strategies to a specific problem. The techniques used here are briefly described below and the interested reader is invited to refer to [40,41] for a broader view.

In the present study, the genome of an individual was defined to contain hourly values of the temperature at the inlet of the ventilated slab (T_{in}) over the time window. Considering that this study focuses on summer conditions, the space search was restricted to a range of temperature defined as:

$$T_{in}(t) \in \left[T_{in,min} : 0.5 : max\left(T_{in,max} ; T_{Outdoor}(t)\right)\right] \quad (24)$$

The lower threshold ($T_{in,min}$) was defined regarding the condensation risk at the inlet of the ventilated slab. The temperature at the surface of concrete on the indoor side should not be lower than 15°C when the indoor conditions are 25 °C and 50 % RH. Because of heat conduction at the very inlet of the slab, the lower threshold was set to 10 °C. The higher threshold was defined in order to limit the research space and, by doing so, the computational time. Considering that cooling was desired most of the time, there would be little benefit in blowing air at temperatures higher than those outdoors during the day, since this would mean that the HVAC would provide heating. It might be necessary, however, during the night, which is the reason why $T_{in,max}$ was set to 25 °C, which was the upper limit for indoor temperature during working hours.

The objective was to minimize the cost function *f*, which takes both the temperature exceedance and the energy demand into account. Penalty coefficients α were added in order to stress the influence of one of the two objectives as follows.

$$f = \alpha_E \, E + \alpha_\theta \, \theta \quad (25)$$

While energy demand does matter and drives a lot of research effort, energy savings are obtained at the cost of larger indoor temperature variations. In modern offices, however, people are used to experiencing a narrow temperature range and indoor temperature remains a key parameter in

technical specifications. As one of the objectives was to demonstrate the ability of the ventilated slab to meet these specifications, it was decided to favour temperature exceedance in this study by using a high value for its penalty coefficient ($\alpha_\theta = 3$) while no penalty was applied to the energy demand ($\alpha_E = 1$).

The first generation for the GA was initialized by means of Latin Hypercube Sampling. Once the cost function had been evaluated, some of the parents were picked randomly to perform selection, then a population of children was generated by performing cross-over. This technique consists of computing a temperature that is included in the range defined by the values of the two parents at the same time. The number of children was the same as the number of parents but some of the parents could be selected multiple times to perform cross-over depending on the value of their cost function. It soon appeared that this technique yielded fast convergence but also poor repeatability, meaning that the GA failed to reach the optimal solution. For this reason, an evolution strategy based on mutations was developed. At the beginning of this strategy, a low mutation rate is applied by resetting a random value of the genome. Then the mutation rate increases, up to a maximum of 20 % of the population, as the efficiency of cross-over decreases. Next, the mutation strategy permutes with three others:

1. Instead of using a random value within the search space, a random draw is performed from a normal distribution. The distribution is centred on the current value and its standard deviation corresponds to 16 % of the range of the search space. This favours the selection of values that narrow the original temperature range;
2. Linear interpolation is performed over the genome at random times and over a random time span. Since the objective is to take advantage of the slab inertia, it is foreseen that the progressive variations at the inlet of the slab should be at least as effective as scattered ones;

3. The time series of the genome is modified by means of a low-pass Gaussian filter using a randomly drawn cut-off frequency. Overall, it generates a time series with a smoothed shape that is similar to the evolution of the outdoor temperature.

The mutation strategy remains the same as long as some of the individuals that have undergone mutation obtain a better cost function than some of the parents. Otherwise, the mutation strategy is changed.

The new generation was obtained by using an elitist strategy and a fixed size for the population of the next generation. Convergence was obtained when the following requirements were met:

1. The cost function of 90 % of the individuals lay within the same range (maximum between ± 2.5 % and ± 0.02);
2. At least 20 generations had been performed;
3. The best individual remained the same for at least 5 generations.

The tuning of a GA is intended to improve its ability to obtain the optimized solution as fast as possible. Besides the evolution strategy, the size of the population, λ, is a key feature that often influences both criteria. It should therefore be tested. Additionally, a repeatability test is convenient to demonstrate the GA's accuracy because of its stochastic nature. Here, the GA was applied 20 times for values of λ that grew from 35 to 80. The optimization was achieved over 24 h for a hot day with high solar loads, so the test was more demanding.

In all cases, the GA was able to find time series for T_{in} such that the temperature exceedance remained at zero. In consequence, the comparison proposed in Figure 22 is based on the energy demand and on the computational time (t_c) only. For the latter, a dimensionless value was preferred in order to provide relative values, as the computational time may vary strongly depending on the machine used. Here, the mean computational time obtained with 35 individuals was used as a reference.

The energy demand remained quite low for all cases (< 0.2 kWh), although it could more than double between the best and the worst solutions. Increasing the number of individuals decreased the discrepancy observed over 20 runs, but the average value did not decrease significantly. However, no clear trend was observed for λ higher than 65. On the other hand, the computational time followed an almost linear trend and tripled when λ doubled. Since this study does not target online control, the computational time is of minor importance and a number of individuals of 65 was maintained for the sake of accuracy.

(a)

(b)

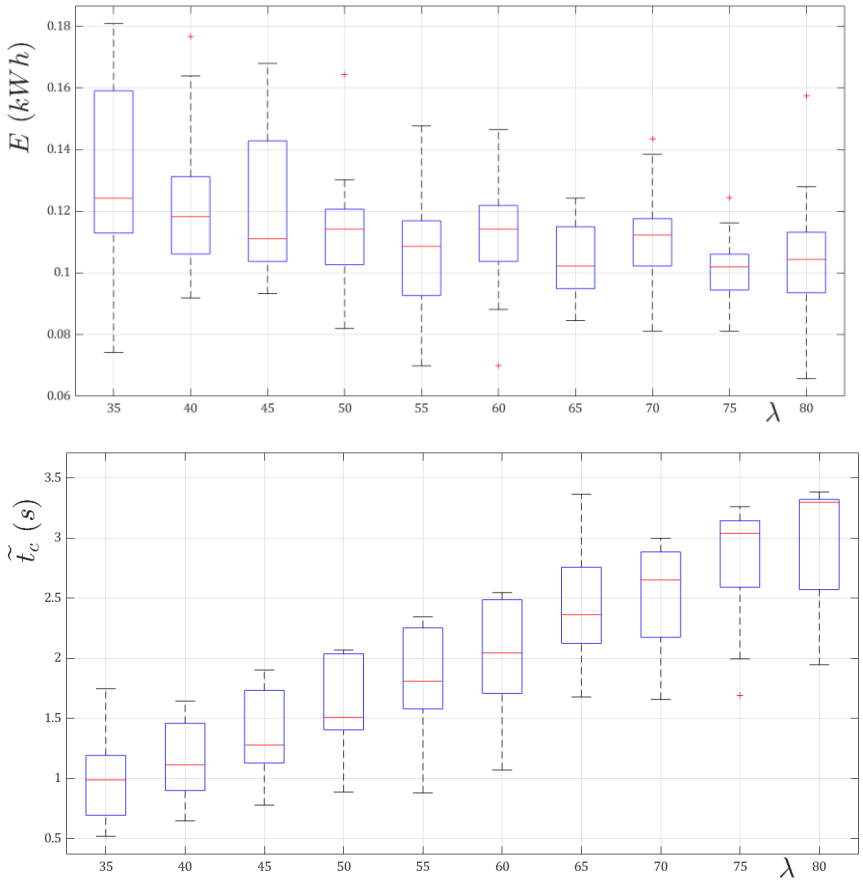

Figure 22: Energy demand (a) and dimensionless computational time t_c (b) obtained from the repeatability test against the size of the population λ for a 24 h long simulation.

8.4. Tuning of model predictive controller

When considering the predictive controller, two key features have to be defined: the time span of the windows and the overlap between two windows. Because of the thermal inertia of the ventilated slab, it is very important to run simulations over a duration that covers most of the settling time of the

system so as to define appropriate values of T_{in}. This also means that the values of T_{in} at the beginning of the time window are determinant because of the impact they have later but this becomes less and less the case as T_{in} comes closer to the end of the time window. To put it another way, there are fewer constraints on the latest values of the genome since their mid-term impact on the room temperature is not simulated. This issue can be overcome by overlapping two consecutive time windows, defined such that:

$$\begin{gathered} Window\ n : t \in \left[t^{j} : t^{j+t_s}\right] \\ Window\ n+1 : t \in \left[t^{j+t_o} : t^{j+t_o+t_s}\right] \\ 0 < t_o < t_s \end{gathered} \tag{26}$$

where t_s is the span of the time window and t_o is the overlap time.

When this is done, only some of the values optimized during the time window *n* are kept while the remaining ones are optimized one more time with the time window *n+1*. The number of values kept and reused depends on the overlap time. It seems safer to use a short overlap time since the optimization will take place more often but this comes at the cost of an increased computational time and an acceptable compromise has to be found. In addition, a reduced search space is used for the time window *n+1*. The objective is to take advantage of the solution obtained with the *n* time window in order to speed up the optimization process.

The influence of t_0 is illustrated in Figure 23 for four values of t_0, 1h being the reference, for a 48h period including a particularly hot day. The optimized values of T_{in} led to satisfactory indoor conditions in all cases. By this, we mean that the temperature exceedance remained null regardless of the overlap time.

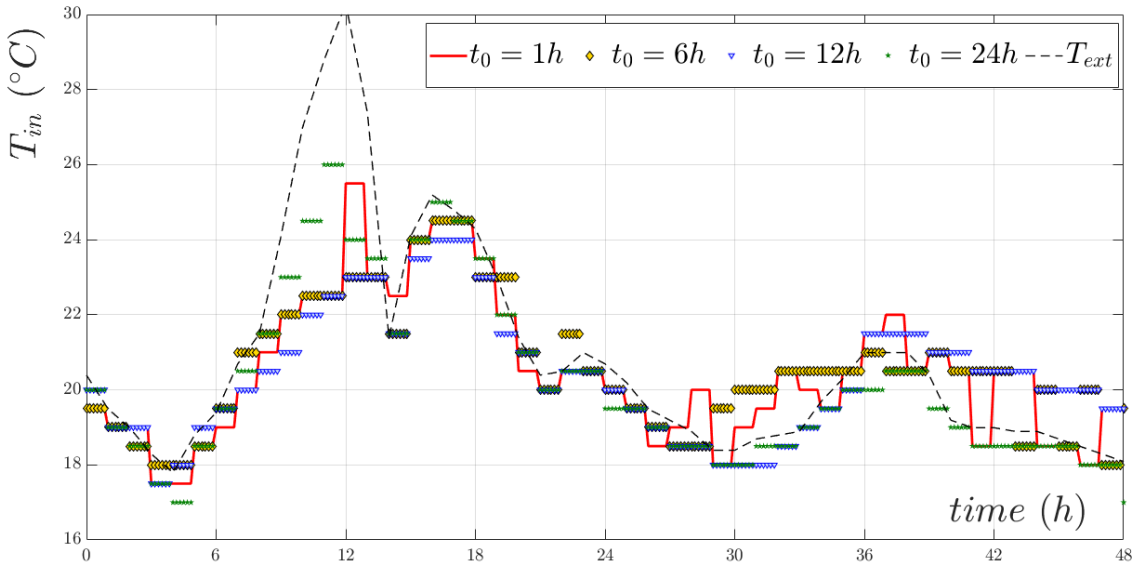

Figure 23: Optimized inlet temperature T_{in} obtained for different values of overlap time t_o over 48h.

For this reason, the analysis mainly focuses on the inlet temperatures T_{in}, which are plotted in Figure 23. The results can be seen to follow the same trend over 48h and the differences remain small (< 2°C) during the night or the second day, when outdoor temperatures remain within a narrow range. Higher differences appear during the first, hot day and can reach 3.5°C. Higher temperatures were particularly obtained with the longer overlap time during this hot period (green stars on Figure 23). However, the trend is shifted on the second day and the values of T_{in} remain lower than with the other overlap times. Our interpretation is that the optimization process took advantage of the thermal inertia provided by the slab on the first day, but it had to be cooled down afterwards. Selecting shorter overlap time led to profiles that remained at a slightly higher temperature during the second day. Such temperatures can be obtained for a lower energy cost by mixing indoor and outdoor airflows. The discrepancies were further analysed by means of three indicators: the Mean Absolute Error (MAE) of the inlet and room temperatures and the Relative Error (RE) of energy demand, as follows:

$$MAE(T_{in}) = \frac{1}{n}\sum_{i=1}^{n}\left|T_{in}(t_i) - T_{in,t_0=1h}(t_i)\right| \quad (27)$$

$$RE(E) = \left| \frac{E - E|_{t_0=1h}}{E|_{t_0=1h}} \right| \quad (28)$$

Here, it should be underlined that the term "error" refers to the difference with respect to the case for which the greatest number of optimizations was performed, assuming that increasing the overlap time cannot lead to better performance levels. The results are presented in Table 4 and clearly show that much lower errors were obtained with an overlap time of 6 hours than with the other two. Therefore, this value was kept for the rest of the study.

Table 4 : Comparison of the errors obtained for different overlap times (t_o = 1h being the reference) for the 48h test presented in Figure 23.

t_0	6h	12h	24h
MAE (T_{in}) (°C)	0.06	0.33	0.17
MAE (T_{room}) (°C)	0.30	1.01	0.77
RE (E) (%)	1.6	35.1	22.1

8.5. State space matrices for the ventilated slab

Matrix	A	B	C	D
6 ACH	$-2.0569\ e^{-5}$ 0 0 0 0 0 0 $-1.4366\ e^{-4}$ 0 0 0 0 0 0 $-2.1106\ e^{-5}$ 0 0 0 0 0 0 $-2.3322\ e^{-5}$ 0 0 0 0 0 0 $-2.1168\ e^{-5}$ 0 0 0 0 0 0 $-8.9924\ e^{-5}$	$1.9201\ e^{-1}$ 0 $1.9202\ e^{-1}$ 0 $1.3950\ e^{-3}$ 0 0 $3.9523\ e^{-3}$ 0 $2.6373\ e^{-3}$ 0 $1.9300\ e^{-3}$	$4.3095\ e^{-5}$ $-6.8696\ e^{-6}$ 0 $-4.7054\ e^{-3}$ 0 0 0 0 $2.4739\ e^{-3}$ 0 $-2.7874\ e^{-3}$ $-2.1352\ e^{-3}$	0 $4.4337\ e^{-1}$	1.1905 1
5 ACH	$-1.9658\ e^{-5}$ 0 0 0 0 0 0 $-1.5290\ e^{-4}$ 0 0 0 0 0 0 $-2.0173\ e^{-5}$ 0 0 0 0 0 0 $-2.2236\ e^{-5}$ 0 0 0 0 0 0 $-2.0228\ e^{-5}$ 0 0 0 0 0 0 $-8.9793\ e^{-5}$	$3.5180\ e^{-1}$ 0 $3.5183\ e^{-1}$ 0 $1.3949\ e^{-3}$ 0 0 $3.9502\ e^{-3}$ 0 $2.6866\ e^{-3}$ 0 $1.9647\ e^{-3}$	$2.3997\ e^{-5}$ $-1.7931\ e^{-6}$ 0 $-5.6329\ e^{-3}$ 0 0 0 0 $2.2789\ e^{-3}$ 0 $-2.8433\ e^{-3}$ $-2.1790\ e^{-3}$	0 $4.2226\ e^{-1}$	1.4260 1
4 ACH	$-1.8711\ e^{-5}$ 0 0 0 0 0 0 $-1.3469\ e^{-4}$ 0 0 0 0 0 0 $-1.9183\ e^{-5}$ 0 0 0 0 0 0 $-2.1056\ e^{-5}$ 0 0 0 0 0 0 $-1.9198\ e^{-5}$ 0 0 0 0 0 0 $-9.0446\ e^{-5}$	$1.9874\ e^{-1}$ 0 $1.9875\ e^{-1}$ 0 $1.2844\ e^{-3}$ 0 0 $3.9462\ e^{-3}$ 0 $2.7373\ e^{-3}$ 0 $2.0097\ e^{-3}$	$4.4708\ e^{-5}$ $-8.0467\ e^{-6}$ 0 $-7.0189\ e^{-3}$ 0 0 0 0 $2.0521\ e^{-3}$ 0 $-2.9006\ e^{-3}$ $-2.2321\ e^{-3}$	0 $3.9942\ e^{-1}$	1.7786 1
3 ACH	$-1.7691\ e^{-5}$ 0 0 0 0 0 0 $-1.4715\ e^{-4}$ 0 0 0 0 0 0 $-1.8177\ e^{-5}$ 0 0 0 0 0 0 $-1.9778\ e^{-5}$ 0 0 0 0 0 0 $-1.8088\ e^{-5}$ 0 0 0 0 0 0 $-8.9088\ e^{-5}$	$3.6271\ e^{-1}$ 0 $3.6273\ e^{-1}$ 0 $1.1884\ e^{-3}$ 0 0 $7.8841\ e^{-3}$ 0 $2.7857\ e^{-3}$ 0 $2.0317\ e^{-3}$	$2.5041\ e^{-5}$ $-2.6066\ e^{-6}$ 0 $-4.6631\ e^{-3}$ 0 0 0 0 $1.7880\ e^{-3}$ 0 $-2.9563\ e^{-3}$ $-2.2657\ e^{-3}$	0 $3.7613\ e^{-1}$	2.3658 1

2 ACH	$-1.6587 e^{-5}$	0	0	0	0	0	$2.0526 e^{-1}$	0	$4.5650 e^{-5}$	$-9.2563 e^{-6}$	0	$-6.9660 e^{-3}$	0	0	0	3.5385
	0	$-1.3016 e^{-4}$	0	0	0	0	$2.0526 e^{-1}$	0								
	0	0	$-1.7219 e^{-5}$	0	0	0	$1.0162 e^{-3}$	0								
	0	0	0	$-1.8357 e^{-5}$	0	0	0	$7.8745 e^{-3}$	0	0	$1.4743 e^{-3}$	0	$-2.9862 e^{-3}$	$-2.2881 e^{-3}$	$3.6271 e^{-1}$	1
	0	0	0	0	$-1.6684 e^{-5}$	0	0	$2.8132 e^{-3}$								
	0	0	0	0	0	$-8.8973 e^{-5}$	0	$2.0508 e^{-3}$								

8.6. State space matrices for the non-ventilated slab (NVS)

Matrix	A				B	C			D
	$-1.4053 e^{-5}$	0	0	0	$2.0741 e^{-4}$	-8.5011	$1.4553 e^{1}$	$-1.5181 e^{1}$	$-1.5321 e^{1}$	$1.5406 e^{2}$
	0	$-2.5571 e^{-4}$	0	0	$-3.5507 e^{-4}$					
	0	0	$-9.2193 e^{-4}$	0	$3.7038 e^{-4}$					
	0	0	0	$-2.0302 e^{-3}$	$3.7381 e^{-4}$					